



INTERNATIONAL UNIVERSITY LIAISON INDONESIA

BACHELOR'S THESIS

**PERFORMANCE REVIEW AND ANALYSIS OF GUAV-190417
TARGET DRONE: AIRFIELDS, SYMMETRIC CLIMB, AND
GLIDING**

By

Jordan Yap Hong Yong

11201701004

Presented to the Faculty of Engineering

In Partial Fulfilment Of the Requirements for the Degree of

SARJANA TEKNIK

In

AVIATION ENGINEERING

FACULTY OF ENGINEERING

BSD City 15345

Indonesia

January 2021

APPROVAL PAGE

PERFORMANCE REVIEW AND ANALYSIS OF GUAV-190417
TARGET DRONE: AIRFIELDS, SYMMETRIC CLIMB, AND
GLIDING

JORDAN YAP HONG YONG

11201701004

Presented to the Faculty of Engineering
In Partial Fulfillment of the Requirements for the Degree of

SARJANA TEKNIK

In

AVIATION ENGINEERING

FACULTY OF ENGINEERING

Triwanto Simanjuntak, PhD

Thesis Advisor



Date 02/03/2021

Dr. Eng. Ressa Octaviany

Thesis Co-Advisor



Date 02/03/2021

Dr. Ir. Prianggada Indra Tanaya, M.M.E.

Dean of Faculty of Engineering

Date

EXAMINER APPROVAL PAGE

Neno Ruseno, S.T, M.Sc

Examiner 1

Date

Ir. Setyo Utomo, M.Sc, M.M

Examiner 2

Date

Assoc. Prof. Chung-Yan Lin, Ph.D.

Examiner 3

Date

ABSTRACT

Performance Review and Analysis of GUAV-190417 Target Drone: Airfields,
Symmetric Climb, and Gliding

by

Jordan Yap Hong Yong

Triwanto Simanjuntak, PhD, Advisor

Dr. Eng. Ressa Octaviany, Co-advisor

In this research, the performance analyses of target drone GUAV-190417 were carried out to assess its performance during take-off, landing, symmetric climb, and gliding. The conceptual and preliminary sizing phase of this target drone were done by the Galaxy Team as a course project in International University Liaison Indonesia (IULI) in 2019. However, the performance analysis at this initial stage of development has not been done yet in which it is essential before proceeding to prototype and production processes. For this study, the geometric parameters and thrust were assumed constant. The aerodynamics characteristic of the drone such as C_L and C_{D_0} were estimated using OpenFOAM v8 with steady laminar flow assumption, that is $C_{L_{\alpha=0}} \sim 0.38$ and $C_{D_0} \sim 0.04$. The results showed that the distances required to take off and airborne are 97.105 m and 114.87 m, respectively. The landing distance with reversed thrust and 50% fuel capacity is 68.314 m. The drone needs 6.67 min to reach 4000 m altitude. The maximum ceiling of the drone is $\sim 16\,000$ m and minimum climbing time to reach this altitude is 60 min. For gliding performance from 4000 m altitude, the gliding time with minimum rate of descent is 13.33 min. By minimizing angle of descent, the gliding range can reach as far as 38.414 km.

Keyword: *UAV, Target Drone, Aerodynamics, Airfield, Climbing, Gliding, Performance Analysis*

ACKNOWLEDGEMENTS

The success and final outcome of this thesis is not the result of my own hard work alone. Of course, with the help and support of the people around, this thesis can be completed duly. I never forget the supports and want to thank all of them sincerely.

First of all, I want to thank **Jesus Christ**, and who has granted countless blessings, knowledge, and opportunities into my thesis writing. Without Him, I will never reach this stage, and I believe all of this is beautiful in His time.

I respect and thank **Triwanto Simanjuntak, Ph.D.** to become my advisor and to provide me an opportunity to do the thesis with him. I will never forget all of his support and guidance. Likewise, he mustered with the time and energy in both academic and non-academic duties, even though he had so many activities and affairs.

I owe my deep gratitude to **Dr. Ressa Octaviany**, a co-advisor and guardian of my class during my studies at IULI. Without great support and encouragement from her, I would not have arrived at this point. The support given is very pronounced, especially in the time management system, which she applies and the information in aerodynamics.

I want to thank deeply **Dr. Ir. Tutuko Prajogo M.S. Mfg. E** as the rector of International University Liaison Indonesia, and **Dr. Ir. Prianggada Indra Tanaya, M.M.E** as the Dean of Faculty Engineering. I will never forget every single support and caring conversation between us.

I would not forget to remember **Neno Rueseno S.T., M.Sc.** as the Head of Aviation Engineering Department and become my lecturer and supporter during the Student Organization activities.

I am thankful for and fortunate enough to get constant encouragement, support, and guidance from **My Beloved Parents and Family**. Likewise, with **Galaxy Team**, consisted of Achmad H., Ezra F., Peter O., and Tazkya R., who worked hard to build this UAV. And not forget, of course, I would like to say many thanks to Celine W., Daniel W.H., Jason Nathanael, Loiza Z., Marcell R., Raihan S., and all my beloved friends who always support and pray for me during this thesis.

Last but not least, I really thank all of the readers who took their time to read this thesis. I hope this thesis can provide benefits and increase your knowledge.

Contents

| | |
|--|------------|
| Approval Page | i |
| Examiner Approval Page | ii |
| Statement by The Author | iii |
| Abstract | iv |
| Acknowledgements | v |
| Contents | vii |
| List of Figures | x |
| List of Tables | xii |
| 1 Introduction | 1 |
| 1.1 Background | 1 |
| 1.1.1 UAV Definition | 1 |
| 1.1.2 Target Drone | 2 |
| 1.2 Target Drone Design by GALAXY TEAM Summary | 3 |
| 1.2.1 Conceptual Design | 3 |
| 1.2.1.1 Benchmarking | 3 |
| 1.2.1.2 Design Configuration | 6 |
| 1.2.2 Preliminary Design | 7 |
| 1.2.2.1 Weight Estimation | 7 |
| 1.2.2.2 Airfoil Selection | 7 |
| 1.2.2.3 GUAV-190417 Characteristic | 11 |

| | | |
|----------|--|-----------|
| 1.2.3 | Design Figure | 11 |
| 1.2.3.1 | 3D View | 11 |
| 1.2.3.2 | Top View | 12 |
| 1.2.3.3 | Side View | 12 |
| 1.2.3.4 | Front View | 12 |
| 1.3 | Problem Statement | 12 |
| 1.4 | Research Purpose | 13 |
| 1.5 | Research Scope | 14 |
| 2 | Literature Review | 16 |
| 2.1 | Equation of Motion | 16 |
| 2.1.1 | Translational motion | 16 |
| 2.2 | Aerodynamics Basis | 18 |
| 2.2.1 | Parabolic lift-drag polar | 18 |
| 2.3 | Airfield Performance | 23 |
| 2.3.1 | Take off ground run | 25 |
| 2.3.2 | The Airborne Phase of The Take Off | 29 |
| 2.3.3 | Landing Ground Run | 33 |
| 2.4 | Climbing Performance | 34 |
| 2.4.1 | Quasi-steady symmetric | 34 |
| 2.5 | Gliding Flight | 38 |
| 3 | Research Methodology | 41 |
| 3.1 | Original Data of GUAV-190417 | 42 |
| 3.2 | Aerodynamic Design Review | 43 |
| 3.3 | Aircraft Aerodynamics Profile | 44 |
| 3.4 | Parabolic Lift Drag Polar | 45 |
| 3.5 | Airfield Performance | 47 |
| 3.5.1 | Take Off Ground Run | 47 |
| 3.5.2 | The Airborne Phase of The Take Off | 48 |
| 3.5.3 | Landing Ground Run | 49 |
| 3.6 | Climbing Performance | 50 |
| 3.7 | Gliding Performance | 53 |

| | | |
|----------|--|-----------|
| 4 | Results and Discussions | 55 |
| 4.1 | Aircraft Characteristic | 55 |
| 4.2 | Aerodynamic Design Review | 55 |
| 4.3 | Airfield Performance | 57 |
| 4.3.1 | Take Off Ground Run | 58 |
| 4.3.2 | Airborne Phase | 59 |
| 4.3.3 | Landing Ground Run | 60 |
| 4.4 | Climbing Performance | 61 |
| 4.5 | Gliding Performance | 64 |
| 5 | Summary, Conclusion, Recommendation | 69 |
| 5.1 | Conclusion | 69 |
| 5.2 | Recommendation | 70 |
| | References | 72 |
| | Appendices | 74 |
| | Turnitin Report | 75 |
| | Curriculum Vitae | 77 |

List of Figures

| | | |
|------|--|----|
| 1.1 | Length to Empty Weight Comparison | 4 |
| 1.2 | Length to Thrust Comparison | 4 |
| 1.3 | Wingspan to Empty Weight Comparison | 5 |
| 1.4 | Wingspan to Thrust Comparison | 5 |
| 1.5 | Weight Factor | 6 |
| 1.6 | Final Configuration | 7 |
| 1.7 | LS-0417 MOD (Mcghee & Beasley, August 1, 1979) | 8 |
| 1.8 | c_l , c_d , and c_m at $Re=6 \times 10^6$ (Mcghee & Beasley, August 1, 1979) . . | 10 |
| 1.9 | Wing Dimension | 11 |
| 1.10 | 3D View | 12 |
| 1.11 | Top View | 13 |
| 1.12 | Side View | 13 |
| 1.13 | Front View | 14 |
| 2.1 | Component of airplane weight along body axis (Ruijgrok, 2009) . . | 18 |
| 2.2 | Force acting on UAV | 24 |
| 2.3 | Take off maneuver (Ruijgrok, 2009) | 25 |
| 2.4 | Takeoff reference speeds for conventional transports(Ruijgrok, 2009) | 26 |
| 2.5 | Balanced field length concept (Ruijgrok, 2009) | 27 |
| 2.6 | Equilibrium of forces during transition | 30 |
| 2.7 | Equilibrium of forces during transition(2) | 31 |
| 2.8 | Schematic for transition to steady climb (Ruijgrok, 2009) | 32 |
| 2.9 | Force acting on UAV during landing | 33 |
| 2.10 | Characteristic of RC and Time Minimum due to Altitude(Ruijgrok, 2009) | 36 |
| 2.11 | Force acting on Gliding Flight | 39 |

| | | |
|------|--|----|
| 3.1 | Major Step | 41 |
| 3.2 | Mesh topology of computational domain | 43 |
| 3.3 | ISA Graph | 51 |
| 4.1 | The pressure contour. | 56 |
| 4.2 | C_D values during iteration | 57 |
| 4.3 | Drag polar of aircraft | 58 |
| 4.4 | Landing distance performance due to Fuel Remaining | 60 |
| 4.5 | Maximum RC Characteristic due to Altitude with 200N Trust Assumption | 61 |
| 4.6 | Maximum RC inverse Characteristic due to Altitude | 63 |
| 4.7 | Minimum Time Needed | 64 |
| 4.8 | GUAV Endurance (Syauqi, 2021) | 65 |
| 4.9 | Performance Diagram | 66 |
| 4.10 | RC Characteristic Due to Velocity in Various Altitude | 67 |
| 4.11 | Gliding Hodograph with 0.1 and 0.3 MTOW | 67 |
| 4.12 | Gliding Hodograph with 0.5 and 0.8 MTOW | 68 |
| 4.13 | Gliding Hodograph MTOW | 68 |

List of Tables

| | | |
|-----|--|----|
| 1.1 | Total Weight Details | 8 |
| 1.2 | Airfoil Coordinates (Mcghee & Beasley, August 1, 1979) | 9 |
| 1.3 | Airfoil Characteristic | 9 |
| 1.4 | Airfoil Characteristic(2) | 10 |
| 1.5 | Wing Dimension | 10 |
| 1.6 | Aircraft Characteristic | 11 |
| | | |
| 4.1 | Wing Characteristic | 55 |
| 4.2 | Wing Characteristic(2) | 56 |
| 4.3 | Performance Variables | 58 |
| 4.4 | Take Off Performance | 59 |
| 4.5 | Airborne Performance | 59 |
| 4.6 | Gliding Performance at 4000 m altitude | 65 |

List of Abbreviations

| | |
|----------------------|--|
| AoA | Angle Of Attack |
| CAD | Computer Aided Design |
| COG | Center Of Gravity |
| C_L | Aircraft Coefficient Of Lift |
| C_D | Aircraft Coefficient Of Drag |
| c_l | Airfoil Coefficient Of Lift |
| c_d | Airfoil Coefficient Of Drag |
| ISA | International Standard Atmosphere |
| LOF | Lift Off |
| MAX | Maximum |
| MIN | Minimum |
| MTOW | Maximum Take Off Weight |
| RC | Rate Of Climb |
| RD | Rate Of Descent |
| UAV | Unmanned Aerial Vehicle |
| UAT | Unmanned Aerial Target |

PERFORMANCE REVIEW AND ANALYSIS OF GUAV-190417 TARGET DRONE:
AIRFIELDS, SYMMETRIC CLIMB, AND GLIDING

Dedicated to my parents

CHAPTER 1

INTRODUCTION

1.1 Background

1.1.1 UAV Definition

Unmanned Aerial Vehicle is a valuable source in the aviation industry nowadays. The definition "Unmanned" defines that the aircraft operation is not requiring any crew or team onboard anymore. The UAV can be controlled by electronic intelligence which is connected by a wireless connection to the ground pilot. By having a very high level of manoeuvrability, flexible deployment and low cost in production and maintenance, UAV has attracted many people to create an innovation and development into it. UAV already implement in many sectors and create a solution in human resource limitation and according to their fields and purposes, UAVs are divided into several categories, such as: (Valavanis, 2014)

- Military roles: Shadowing the opponent armada, Decoying missiles, Relaying radio signals, Surveillance and Target drone.
- Agriculture: Monitoring and spraying
- Lifeguard: Search and rescue in beach and hiking area
- Natural Authorities: Heat and water level monitoring
- Photography: Mapping, capture and video making
- Police Authorities: Security and searching

With so many different sectors and purposes, UAV sizes are categorized into various types, the division of this type is to adjust the size to their function. This division

generates them to achieve their goals with a higher level of effectiveness. Those types are:

1. High Altitude Long Endurance (HALE)

A type which has a 35 m wingspan that supports over 15 000 m for altitude and having endurance for more than 24 h. On army purposes, they use it to scout and watch the enemy/threat from a distance (trans-global). This aircraft is also equipped with many weapons. The Air Force only carries out the operation of this UAV from a fixed base.

2. Medium Altitude Long Endurance (MALE)

This type flies to a distance of 5000 m until 15 000 m, and the endurance reaches 24 h. However, the control range of this aircraft is smaller than HALE, the range from fixed bases is only around 500 km.

3. Medium Range or Tactical UAV (TUAV)

This type is a simpler and smaller type of aircraft than HALE and MALE. It can only be controlled 100 to 300 km.

4. Mini UAV (MUAV)

A mini type of UAV which has a certain weight below 20 kg, the operating system can be implemented up to 30 kg.

5. Micro UAV (MAV)

The UAV type only has less than 150 mm for the wingspan. Because it is very small, the atmosphere's turbulence is very easy to occur in this UAV. All types of MUAV often experience problems with precipitation. Therefore, this type is only used in cities and closed rooms.

6. Nano-Air Vehicle (NAV)

The smallest type of UAV with a sycamore seed size with 40 mm wingspan, this UAV is used to mess up radar confusion.

1.1.2 Target Drone

Target drone or Unmanned Aerial Target (UAT) is also a part of UAV. In the 1910s, the target drones were first used in the Vietnam War on a wide scale. In various

new functions, such as serving as decoys in battle, firing rockets and missiles at fixed objectives, and delivering leaflets for psychological operations, drones have even started to be used. Nevertheless, it is mandatory to give this drone great versatility for its successful usage on current military needs to simulate today's challenges that might face the soldiers being educated and trained. As the times progressed, target drone continued to be developed. They began installing the MDI (Miss Distance Indicator), developed its maneuverability, and replaced the propeller with a jet engine. This aims to get better and more sophisticated drone target performance.

1.2 Target Drone Design by GALAXY TEAM Summary

Galaxy Team is a group under the university that is developing and aspiring to create a subsonic target drone. Their target drong was named GUAV-190417. In the GUAV-190417 design they applied engineering design steps to realize the final design result. The steps start from Conceptual design, Preliminary Design, Detail Design, Performance Analysis, Prototype, Producing and Testing. The data obtained from the Galaxy Team such as:

1.2.1 Conceptual Design

1.2.1.1 Benchmarking

The results of these benchmarking were obtained from several sources of companies that have succeeded in producing UAT. The results of this benchmarking compare several characteristics, such as:

- Length to Empty Weight Comparison

It can be seen in Figure 1.1, the majority of the aircraft designed have a fuselage length of 2 m - 4 m with an empty weight below 2000 N.

- Length to Thrust Comparison

For comparison of the thrust itself. The Figure 1.2 shows that the majority

PERFORMANCE REVIEW AND ANALYSIS OF GUAUV-190417 TARGET DRONE:
AIRFIELDS, SYMMETRIC CLIMB, AND GLIDING

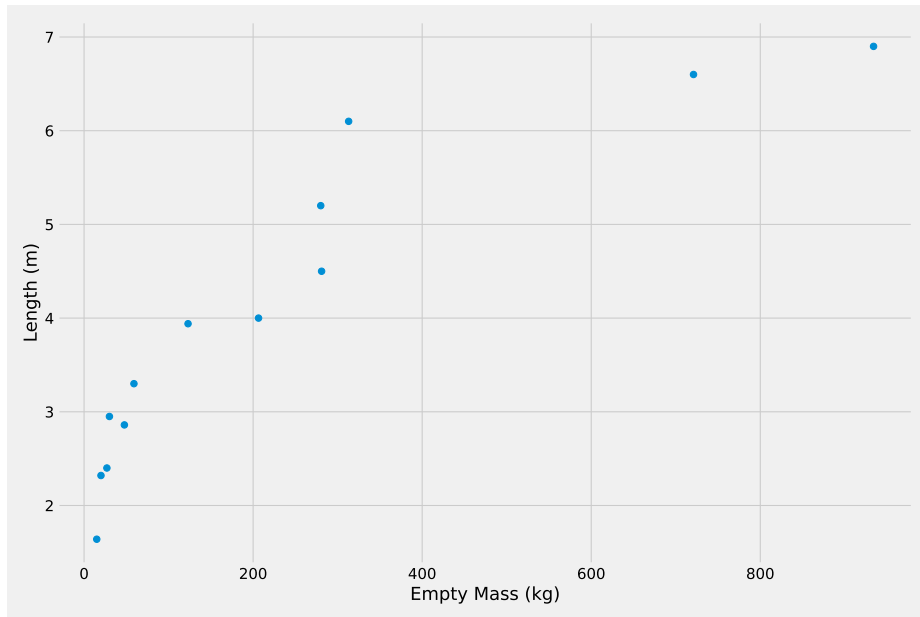


FIGURE 1.1: Length to Empty Weight Comparison

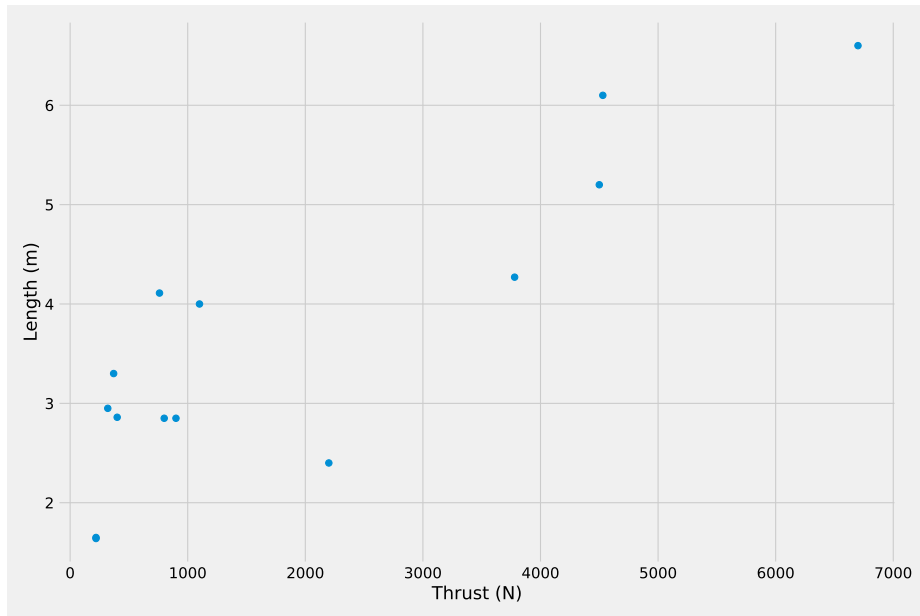


FIGURE 1.2: Length to Thrust Comparison

of Target Drone UAVs with 2 m - 4 m fuselage lengths have thrusts below 1000 N.

- Wingspan to Empty Weight Comparison

PERFORMANCE REVIEW AND ANALYSIS OF GUAV-190417 TARGET DRONE:
AIRFIELDS, SYMMETRIC CLIMB, AND GLIDING

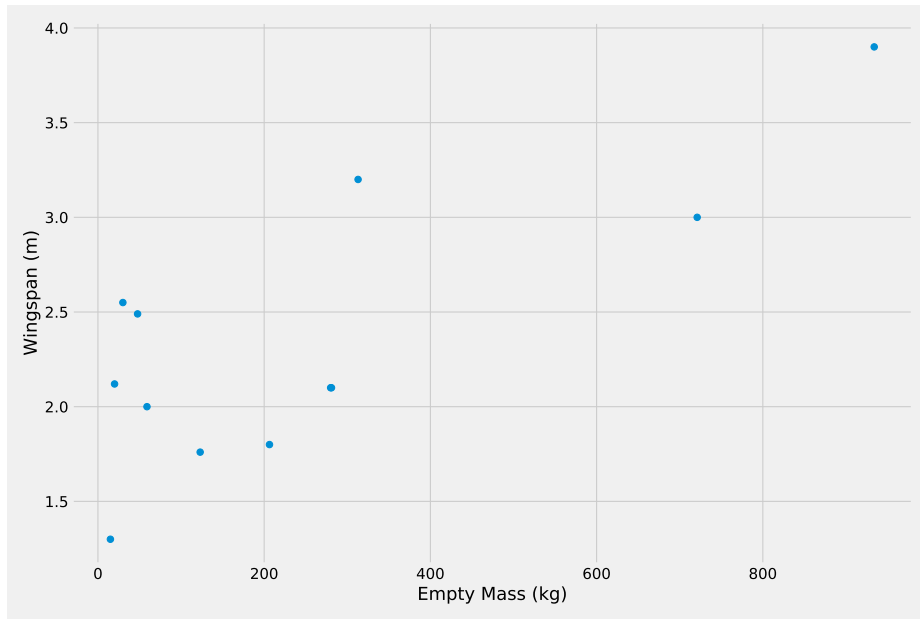


FIGURE 1.3: Wingspan to Empty Weight Comparison

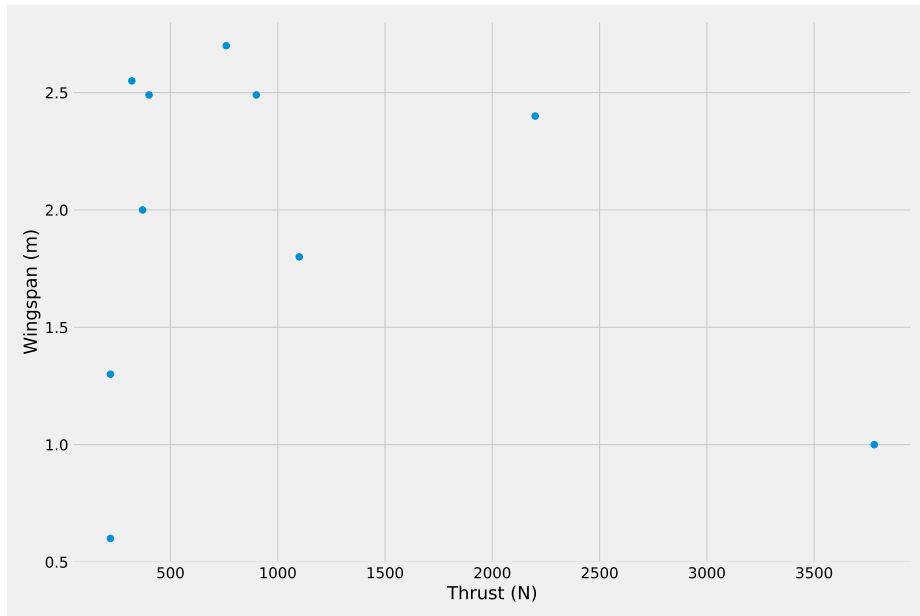


FIGURE 1.4: Wingspan to Thrust Comparison

In the UAV target drone benchmark Figure 1.3, the majority wingspan used is between 1.5 m - 3 m with an empty weight below 2000 N.

- Wingspan to Thrust Comparison

With a 1.5 m - 3 m wingspan they mostly use Thrust below 1000 N in Figure 1.4

Given the overview of this benchmark, Galaxy Team decided to build a Target Drone UAV with a size of approximately 2 m for the wingspan and 3 m for the fuselage length. This is also influenced by the thrust factor of the jet engine that will be used, which is 250 N - 300 N.

1.2.1.2 Design Configuration

Design Configuration is a step in the design used to determine the fixed components to be used in the final design. These components include the aircraft body type, wing type, landing gear, etc. Because each component has its variety, Galaxy Team use a weight factor and scoring system to determine it. (Nicolai, 2010) The weight factor method is then used to determine which classification you want to maximize and minimize. From each existing class, a percentage determination is also needed. In the GUAV-190417 design, Galaxy Team set 50% on maximization, which is focusing on reliability, performance and producibility. And for the minimization, they are focusing on cost, then weight. The Figure 1.5 give a more detail understanding. By creating 5 design configurations based on Reliability, Per-

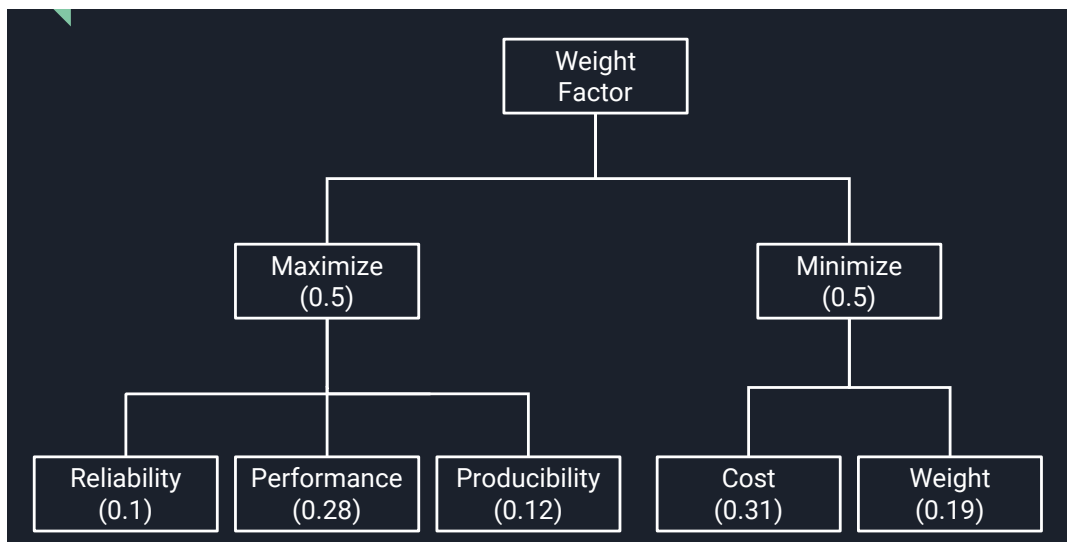
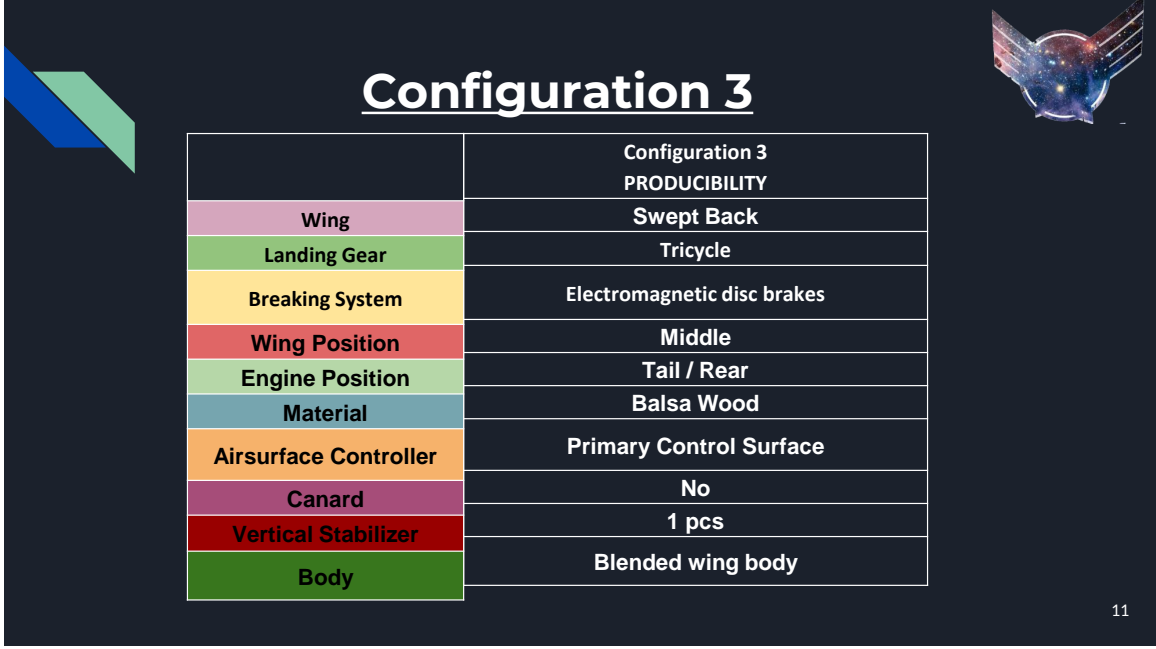


FIGURE 1.5: Weight Factor

formance, Producibility, Weight and Cost classification. The configuration 3 with

Producibility Classification will be used for the final design. The Figure 1.6 shows the final configuration.



Configuration 3

| | Configuration 3 PRODUCIBILITY |
|-----------------------|----------------------------------|
| Wing | Swept Back |
| Landing Gear | Tricycle |
| Breaking System | Electromagnetic disc brakes |
| Wing Position | Middle |
| Engine Position | Tail / Rear |
| Material | Balsa Wood |
| Airsurface Controller | Primary Control Surface |
| Canard | No |
| Vertical Stabilizer | 1 pcs |
| Body | Blended wing body |

11

FIGURE 1.6: Final Configuration

1.2.2 Preliminary Design

1.2.2.1 Weight Estimation

The total weight estimation of this target drone is estimated by summing up all the weight in every component. To anticipate the unpredictable and missing part weight, the total weight must added by 25% from the total estimation to become the additional weight. The components of weight detail will be shown on Table 1.1.

From the calculation, we can conclude that the GUAV-190417s total weight is 35kg = 343N.

1.2.2.2 Airfoil Selection

To produce a lift force, a proper airfoil type is needed. The lift coefficient value and the high possibility to be built are the most important to be considered. That's

TABLE 1.1: Total Weight Details

| No | Item | Weight (kg) |
|------------------|----------------------------------|-------------|
| 1. | Engine | 5 |
| 2. | Fuel | 8 |
| 3. | Fuel Tank | 0.4 |
| 4. | Body | 12 |
| | Wing | |
| | Elevon | |
| | Vertical & Horizontal Stabilizer | |
| 5. | Brakes | 0.1 |
| 6. | Landing Gear | 0.5 |
| 7. | Wire | 0.02 |
| 8. | Servo | 0.2 |
| 9. | MDI | 2 |
| Total Estimation | | 28.22 |
| Additional (25%) | | 6.78 |
| Total Weight | | 35 |

why we applied the LS(1)-0417 MOD airfoil type in GUAV-200417. The Figure 1.7 shows the shape and Table 1.2 shows the airfoil coordinates.

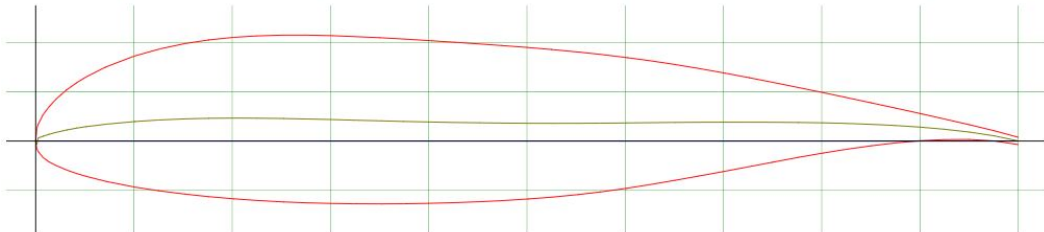


FIGURE 1.7: LS-0417 MOD (Mcghee & Beasley, August 1, 1979)

Table 1.3 shows the characteristic of LS-0417 MOD airfoil. Those variables will be use to find the other aircraft characteristics, for example lift coefficient on airfoil and wing and etc. From Figure 1.8 section A, the variables related to lift coefficient can be found, as well as for section B and C. The variables and their values can be seen in the Table 1.4. Figure 1.9 shows the detail dimensioning of

PERFORMANCE REVIEW AND ANALYSIS OF GUAV-190417 TARGET DRONE:
AIRFIELDS, SYMMETRIC CLIMB, AND GLIDING

TABLE 1.2: Airfoil Coordinates (Mcghee & Beasley, August 1, 1979)

| Upper Surface | | | | Lower Surface | | | |
|---------------|---------|-------------|-------------|---------------|----------|-------------|-------------|
| X-Axis | Y-Axis | (Continued) | (Continued) | X-Axis | Y-Axis | (Continued) | (Continued) |
| 0 | 0 | 0.47432 | 0.0968 | 0 | 0 | 0.47321 | -0.06042 |
| 0.00124 | 0.01286 | 0.49983 | 0.09488 | 0.00106 | -0.00728 | 0.50145 | -0.05869 |
| 0.00239 | 0.01665 | 0.52478 | 0.0929 | 0.00248 | -0.01063 | 0.52561 | -0.05681 |
| 0.00741 | 0.02642 | 0.55306 | 0.09013 | 0.00765 | -0.01683 | 0.55215 | -0.05424 |
| 0.013 | 0.03408 | 0.57414 | 0.08788 | 0.01338 | -0.02096 | 0.57495 | -0.05155 |
| 0.02088 | 0.04266 | 0.6025 | 0.08445 | 0.01991 | -0.02441 | 0.60089 | -0.04793 |
| 0.03133 | 0.0517 | 0.62408 | 0.08153 | 0.03183 | -0.02945 | 0.62389 | -0.04432 |
| 0.0415 | 0.05894 | 0.64961 | 0.0777 | 0.04187 | -0.03294 | 0.6507 | -0.03976 |
| 0.0508 | 0.06464 | 0.67575 | 0.07399 | 0.0511 | -0.03573 | 0.67458 | -0.03552 |
| 0.07102 | 0.07488 | 0.7024 | 0.06864 | 0.07203 | -0.04101 | 0.69911 | -0.03104 |
| 0.09992 | 0.08593 | 0.72617 | 0.06416 | 0.10088 | -0.04665 | 0.72419 | -0.02632 |
| 0.12642 | 0.09341 | 0.74966 | 0.05956 | 0.12531 | -0.0504 | 0.74967 | -0.02148 |
| 0.15195 | 0.09875 | 0.77674 | 0.05412 | 0.15156 | -0.05374 | 0.77634 | -0.01652 |
| 0.17613 | 0.10242 | 0.80302 | 0.0487 | 0.17603 | -0.05633 | 0.80123 | -0.01216 |
| 0.20136 | 0.10503 | 0.82446 | 0.04422 | 0.20151 | -0.05851 | 0.8248 | -0.00841 |
| 0.22458 | 0.10651 | 0.85023 | 0.03874 | 0.22487 | -0.06016 | 0.85026 | -0.00485 |
| 0.25191 | 0.10731 | 0.87503 | 0.03337 | 0.25229 | -0.06167 | 0.87444 | -0.00195 |
| 0.27462 | 0.10734 | 0.90244 | 0.02737 | 0.27686 | -0.06259 | 0.90007 | 0.00032 |
| 0.30195 | 0.10678 | 0.92463 | 0.02338 | 0.3018 | -0.06323 | 0.92418 | 0.00147 |
| 0.32382 | 0.10597 | 0.95022 | 0.01657 | 0.3233 | -0.06355 | 0.95022 | 0.0016 |
| 0.35017 | 0.10471 | 0.97593 | 0.01034 | 0.35239 | -0.06367 | 0.97586 | 0.00013 |
| 0.37685 | 0.1032 | 1 | 0.00378 | 0.37431 | -0.06353 | 1 | -0.00354 |
| 0.40344 | 0.10157 | 1.01 | 0 | 0.4 | -0.06312 | 1.03 | -0.0045 |
| 0.42607 | 0.10012 | 1.02 | -0.003 | 0.4258 | -0.06243 | N/A | N/A |
| 0.45228 | 0.09836 | 1.03 | -0.0045 | 0.45148 | -0.06146 | N/A | N/A |

TABLE 1.3: Airfoil Characteristic

| Variable | Value | Unit |
|-------------------------------------|---------|------|
| Maximum airfoil thickness | 0.17c | |
| α at $c_l = 0$ | -4 | deg |
| c_{l_α} | 6.3814 | /rad |
| c_{m_α} for $\alpha > 6$ deg | 0.2455 | /rad |
| c_{m_α} for $\alpha < 4$ deg | -0.1705 | /rad |

PERFORMANCE REVIEW AND ANALYSIS OF GUAV-190417 TARGET DRONE:
AIRFIELDS, SYMMETRIC CLIMB, AND GLIDING

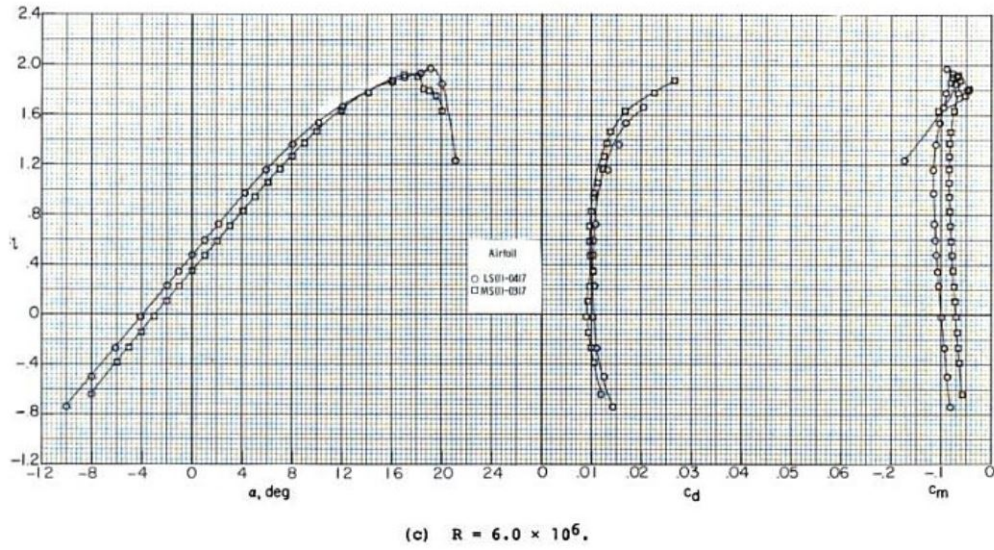


FIGURE 1.8: c_l , c_d , and c_m at $Re=6 \times 10^6$ (Mcghee & Beasley, August 1, 1979)

TABLE 1.4: Airfoil Characteristic(2)

| Variable | Value | Unit |
|----------------|-------|------|
| α_{max} | 17 | deg |
| $c_{l_{max}}$ | 1.95 | |

GUAV swept back wing type from tow view. And Table 1.5 shows the details of wing dimensioning.

TABLE 1.5: Wing Dimension

| Variable | Value | Unit |
|--------------------------|---------|-------|
| Wingspan | 1.916 | m |
| Chord tip | 0.05913 | m |
| Chord root | 0.57875 | m |
| Swept angle UPPER | 30 | deg |
| Swept angle LOWER | 10 | deg |
| Swept angle mean to mean | 20.65 | deg |
| Gross area | 0.48135 | m^2 |

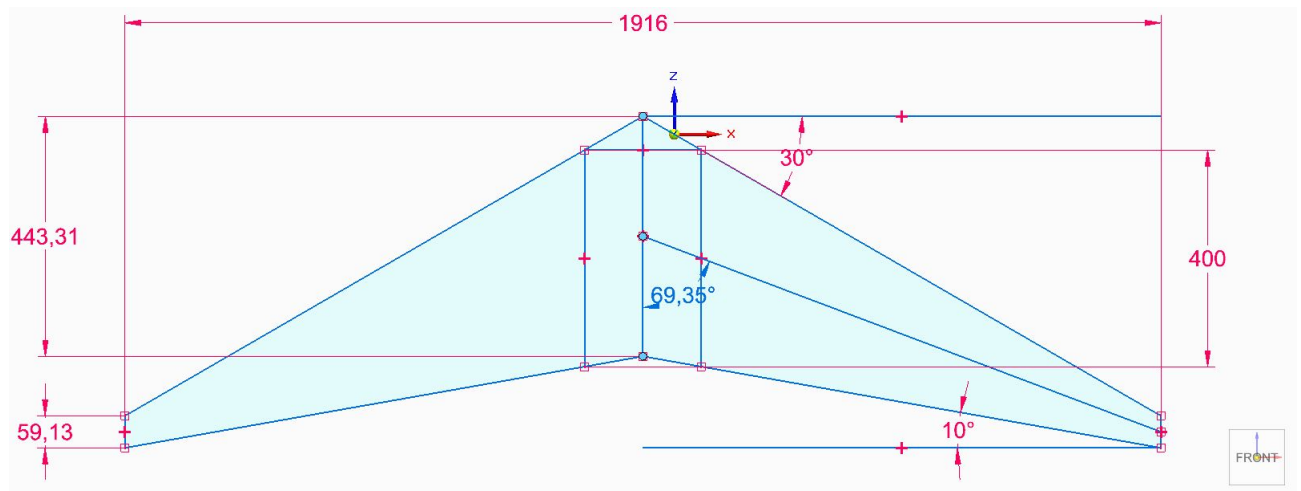


FIGURE 1.9: Wing Dimension

1.2.2.3 GUAV-190417 Characteristic

In Table 1.6, Galaxy Team is showing their aircraft and engine characteristic.

TABLE 1.6: Aircraft Characteristic

| Variable | Value | Unit |
|----------------|-------------|-------------------|
| Weight | 343 | N |
| Mach | 0.3 | |
| Rho ρ | 1.225 | kg/m ³ |
| Velocity | 103.2 | m/s |
| Thrust max | 250 | N |
| Viscosity | 0.00001789 | kg/m/s |
| Mass fuel rate | 0.01019 | |
| C_T | 0.000399448 | 1/s |

1.2.3 Design Figure

1.2.3.1 3D View

Figure 1.10 shows GUAV-190417 design in 3D view with x, y, and z-axis.

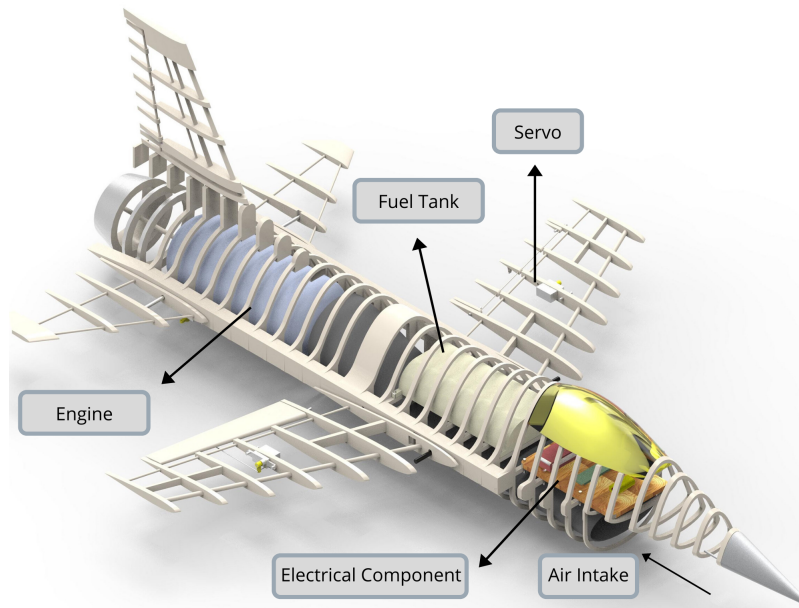


FIGURE 1.10: 3D View

1.2.3.2 Top View

The view of GUAV-190417 in x-axis and z-axis can be seen in Figure 1.11.

1.2.3.3 Side View

The view of GUAV-190417 in x-axis and y-axis can be seen in Figure 1.12.

1.2.3.4 Front View

The view of GUAV-190417 in y-axis and z-axis can be seen in Figure 1.13

1.3 Problem Statement

- Performance Analysis and Review

The target drone GUAV-190417 has been completed in the preliminary sizing. However, the performance of target drone has not been analyzed till this day. In this condition, the prototype, production, and testing can not be continued.

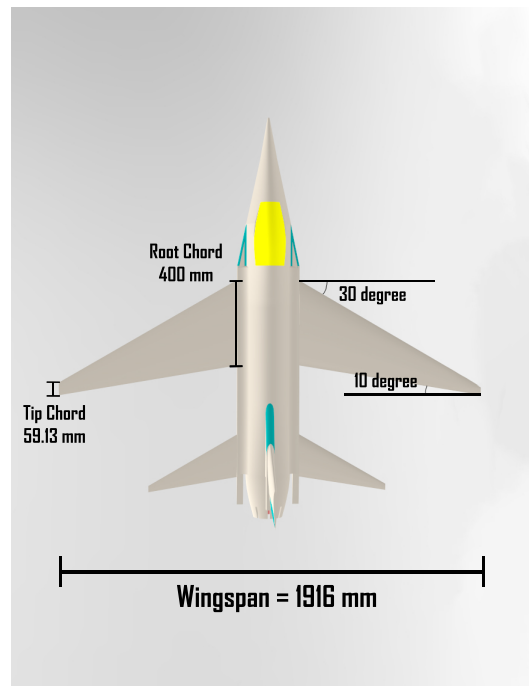


FIGURE 1.11: Top View

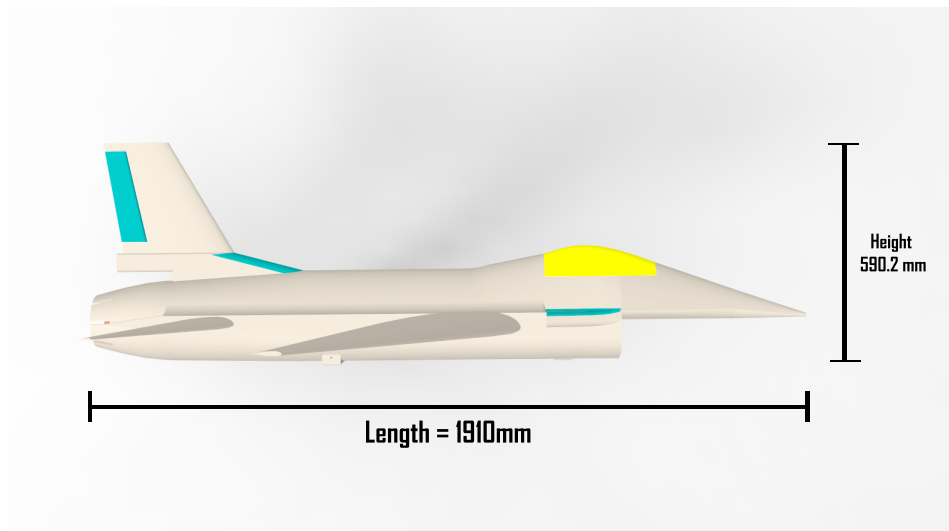


FIGURE 1.12: Side View

1.4 Research Purpose

The purposes of this work are to analyze and review the GUAV-190417 preliminary sizing by calculating:

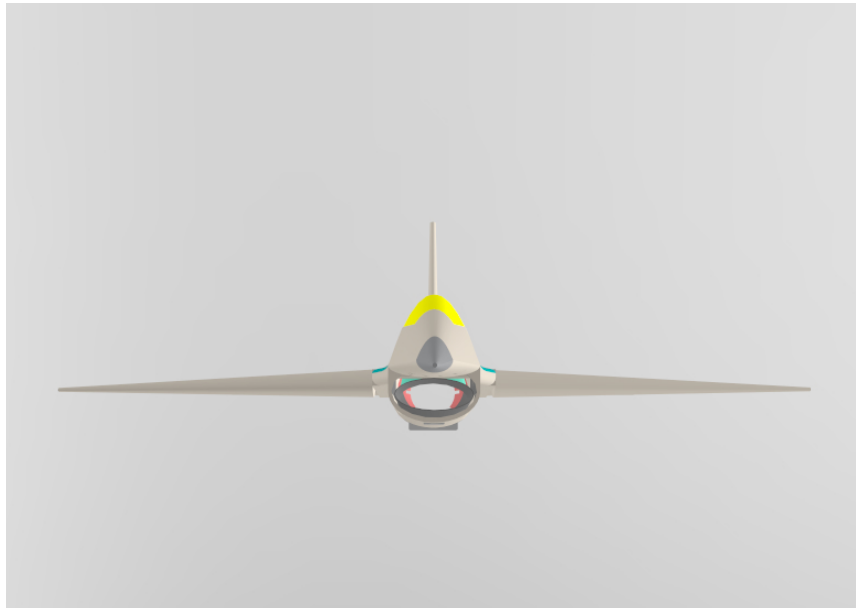


FIGURE 1.13: Front View

- The lift coefficient, drag coefficient and lift drag polar coefficient using Open-FOAM software and manual calculation.
- The airfield performance in terms of take off ground run distance, transition distance during the airborne phase, and landing distance.
- The symmetric climbing performance regarding the absolute ceilings, fuel used and time required at different altitudes.
- The gliding performance concerning the rate of descent, time maximum and range maximum at different lift coefficients.

1.5 Research Scope

- Galaxy Team - GUAV-190417 Target Drone design is applied in this work. In reality, the weight estimation will vary until the target drone is manufactured. The performance may impact the actual weight.
- A single jet engine of GUAV-190417 by Galaxy Team is installed with thrust power and mass fuel rate.

- In reality, the aircraft cant maintain their altitude exactly in a steady altitude condition. They sometimes have to adjust because of perturbations. In this work, we assume the UAV is flying at a steady altitude condition.
- In aircraft efficiency, the impact of elements such as weather events is not taken into consideration.
- As long as the analysis is followed and derived from the current literature, the limitations of the analytical reliability, estimation, and formula of aerodynamic relationships may remain.
- Taking into consideration the time for the completion of this work, the consistency of the analysis could be influenced directly or indirectly.
- This work only considered Airfield, Symmetric Climb, and Gliding performance. More detailed information about the performance knowledge and analysis can be found by combining the data and result with (Syauqi, 2021).

CHAPTER 2

LITERATURE REVIEW

2.1 Equation of Motion

2.1.1 Translational motion

In the translational motion of an aircraft, Newton's second law of motion still applies. The object will be affected by external forces and will produce the resultant Force, which is denoted by F . The equation shown as:

$$\vec{F} = \frac{d(M\vec{V})}{dt} \quad (2.1)$$

M is the total mass of aircraft consisting of body, fuel, and another payload. And v itself is the linear velocity vector. Aircraft is assumed to be a rigid body with constant mass. Newton's second law would be:

$$\begin{aligned} \vec{F} &= M \frac{d\vec{V}}{dt} \\ &= M\vec{a} \end{aligned} \quad (2.2)$$

Because v is a vector, the vector consists of velocity vector derivative due to time and angular velocity. So the equation is shown as:

$$\vec{F} = M \left(\frac{\delta\vec{V}}{\delta t} + \vec{\Omega} \times \vec{V} \right) \quad (2.3)$$

There are 3 unit vectors to determine the direction in 3 axes. I for x-axis direction, J for y-axis and K for the z-axis. For each value they will be written as:

$$\begin{aligned}\vec{V} &= u\vec{i} + v\vec{j} + w\vec{k} \\ \vec{\Omega} &= p\vec{i} + q\vec{j} + r\vec{k}\end{aligned}\tag{2.4}$$

The total Force will become:

$$F = F_x\vec{i} + F_y\vec{j} + F_z\vec{k}\tag{2.5}$$

Where,

$$\begin{aligned}F_x &= M \left(\frac{du}{dt} + wq - vr \right) \\ F_y &= M \left(\frac{dv}{dt} + ur - wp \right) \\ F_z &= M \left(\frac{dw}{dt} + vp - uq \right)\end{aligned}\tag{2.6}$$

For total force, it consists of resultant aerodynamic force and weight. Where for the aerodynamic resultant, it includes of aerodynamic force and trust:

$$\begin{aligned}\vec{F} &= \vec{A} + \vec{W} \\ &= (\vec{R} + \vec{T}) + \vec{W}\end{aligned}\tag{2.7}$$

Refer to Fig 2.1, since the weight is not parallel with the body axis (create an angle from everybody axes). The weight along the body axes are:

$$\begin{aligned}W_x &= -W \sin\theta \\ W_y &= W \cos\theta \sin\Phi \\ W_z &= W \cos\theta \cos\Phi\end{aligned}\tag{2.8}$$

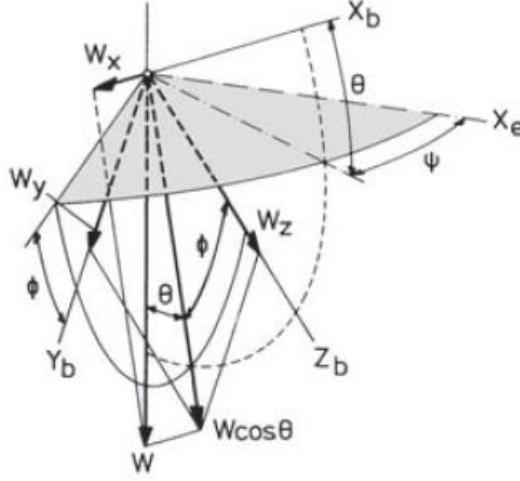


FIGURE 2.1: Component of airplane weight along body axis (Ruijgrok, 2009)

So by substituting equation 2.6 and 2.8 to 2.7, the equation will become:

$$\begin{aligned}
 M \left(\frac{du}{dt} + wq - vr \right) &= -W \sin\theta + A_x \\
 M \left(\frac{dv}{dt} + ur - wp \right) &= W \cos\theta \sin\Phi + A_y \\
 M \left(\frac{dw}{dt} + vp - uq \right) &= W \cos\theta \cos\Phi + A_z
 \end{aligned} \tag{2.9}$$

Where A_x , A_y and A_z are the resultant of aerodynamic Force in scalar value (Ruijgrok, 2009).

2.2 Aerodynamics Basis

2.2.1 Parabolic lift-drag polar

The aircraft's total drag can be split into several sections, and those happen because the drag occurs in every component are having a different value. We can write the

total drag: (J. Anderson, 2011)

$$D = D_W + D_n \quad (2.10)$$

As we know the wing drag consists of induced drag and profile drag, the equation can be modified to:

$$D = D_i + D_p + D_n \quad (2.11)$$

Induced drag is the drag force produced by the lift force, so when the lift force increases, the drag force will also be produced. For the subsonic airspeed with Mach < 1 , the wave drag force will be equal to zero. The drag of the aircraft components is often generated by pressure drag, skin friction drag and wave drag combined. And because of D_n represents several different components, the C_{Dn} will also impact by different surface areas S_n , so that the equation will be shown:

$$C_D \frac{1}{2} \rho v^2 S = C_{Di} \frac{1}{2} v^2 \rho S + C_{Dp} \frac{1}{2} v^2 \rho S + (\Sigma C_{Dn} S_n) \frac{1}{2} \rho V^2 \quad (2.12)$$

By eliminating the same variable from both sides, the equation becomes:

$$C_D = C_{Di} + C_{Dp} + \frac{\Sigma C_{Dn} S_n}{S} \quad (2.13)$$

The lift coefficient's not the only one who affected the induced drag coefficient, but the Aspect Ratio, π and wing efficiency factor also impact it. The wing efficiency factor indicates the elliptical spanwise lift distribution, which acts on the wing. This makes the elliptic lift distribution value is equal to 1, and for the other spanwise lift distribution shape, the value will be less than 1.

$$C_D = \frac{C_L^2}{\pi AR \phi} + C_{Dp} + \frac{\Sigma C_{Dn} S_n}{S} \quad (2.14)$$

Because the angle of attack affects the profile and parasite drag coefficient, the equation becomes:

$$C_D = \frac{C_L^2}{\pi AR \phi} + X C_L^2 + \left[C_{Dp} + \frac{\Sigma C_{Dn} S_n}{S} \right]_{C_L=0} \quad (2.15)$$

Where Oswald's efficiency factor written as

$$\frac{1}{e} = X\pi AR + \frac{1}{\phi} \quad (2.16)$$

And the term of XC_L^2 represents the assumed parabolic change of the profile and parasite drag coefficients with lift coefficient. The quantity in parentheses is termed a zero-lift drag coefficient, and the symbol becomes C_{D_o} . Then, equation 2.15 can be transformed into:

$$C_D = C_{D_o} + \frac{C_L^2}{\pi ARe} \quad (2.17)$$

To simplify the equation, the 'k' induced drag factor can be written for $1/(\pi ARe)$.

$$C_D = C_{D_o} + kC_L^2 \quad (2.18)$$

At transonic airspeed with Mach = 1 and supersonic airspeed with Mach > 1, the parabolic lift-drag polar also can be applied, in terms that the polar drag coefficient and induced drag factor must be adjusted. In expectation of later discussions, it should be remembered that aircraft efficiency is calculated in certain ways. Especially in the maximum aerodynamics ratio, such as C_L/C_D , C_L^3/C_D^2 and C_L/C_D^2 (McCormick, 1994).

To get the maximum value of C_L/C_D , we must differentiate C_L/C_D respect to C_L and equates to zero.

1st step:

$$\begin{aligned} \left(\frac{C_L}{C_D}\right)_{MAX} &= \frac{d(C_L/C_D)}{dC_L} = 0 \\ &= \frac{\frac{dC_L}{dC_L}C_D - C_L \frac{dC_D}{dC_L}}{C_D^2} = 0 \\ &= C_D - C_L \frac{dC_D}{dC_L} = 0 \end{aligned} \quad (2.19)$$

$$C_D = C_L \frac{dC_D}{dC_L}$$

$$\frac{dC_D}{dC_L} = \frac{C_D}{C_L}$$

2nd step: Where,

$$\begin{aligned}
 C_D &= C_{D_o} + kC_L^2 \\
 C_D &= C_{D_o} + \frac{C_L^2}{\pi A Re} \\
 \frac{dC_D}{dC_L} &= 0 + \frac{2C_L}{\pi A Re}
 \end{aligned} \tag{2.20}$$

3rd step: Substitute equation 2.19 and 2.20, we will get:

$$\begin{aligned}
 \frac{C_D}{C_L} &= \frac{2C_L}{\pi A Re} \\
 2C_L^2 &= \pi A Re C_D \\
 2C_L^2 &= \pi A Re \left(C_{D_o} + \frac{C_L^2}{\pi A Re} \right) \\
 2C_L^2 &= \pi A Re C_{D_o} + C_L^2 \\
 C_L^2 &= \pi A Re C_{D_o} \\
 C_L &= \sqrt{\pi A Re C_{D_o}}
 \end{aligned} \tag{2.21}$$

4th step: Substitute equation 2.21 to 2.18

$$\begin{aligned}
 C_D &= C_{D_o} + \frac{(\sqrt{\pi A Re C_{D_o}})^2}{\pi A Re} \\
 C_D &= C_{D_o} + C_{D_o} \\
 C_D &= 2C_{D_o}
 \end{aligned} \tag{2.22}$$

5th(FINAL) step: Substitute equation 2.21 and 2.22

$$\begin{aligned}
 \left(\frac{C_L}{C_D} \right)_{MAX} &= \frac{C_L}{C_D} \\
 &= \frac{\sqrt{\pi A Re C_{D_o}}}{2C_{D_o}} \\
 &= \frac{1}{2} \frac{\sqrt{\pi A Re}}{\sqrt{C_{D_o}}} \\
 &= \frac{1}{2} \sqrt{\frac{\pi A Re}{C_{D_o}}}
 \end{aligned} \tag{2.23}$$

To get the maximum value of C_L^3/C_D^2 , we must differentiate C_L^3/C_D^2 respect to C_L and equates to zero. By following the steps:

1st step: Differentiate C_L^3/C_D^2 respect to C_L

$$\frac{dC_D}{dC_L} = \frac{3C_D}{2C_L} \quad (2.24)$$

2nd step: Differentiate C_D respect to C_L

$$\frac{dC_D}{dC_L} = \frac{2C_L}{\pi A Re} \quad (2.25)$$

3rd step: Substitute equation 2.24 to 2.25

$$C_L = \sqrt{3C_{D_o}\pi A Re} \quad (2.26)$$

4th step: Substitute equation 2.26 to 2.18

$$C_D = 4C_{D_o} \quad (2.27)$$

5th(FINAL) step: Substitute equation 2.26 and 2.27 to C_L^3/C_D^2

$$\left(\frac{C_L^3}{C_D^2}\right)_{MAX} = \frac{3\sqrt{3}}{16}\pi A Re \sqrt{\frac{\pi A Re}{C_{D_o}}} \quad (2.28)$$

To get the maximum value of C_L/C_D^2 , we must differentiate C_L/C_D^2 respect to C_L and equates to zero.

1st step: Differentiate C_L/C_D^2 respect to C_L

$$\frac{dC_D}{dC_L} = \frac{C_D}{2C_L} \quad (2.29)$$

2nd step: Differentiate C_D respect to C_L

$$\frac{dC_D}{dC_L} = \frac{2C_L}{\pi A Re} \quad (2.30)$$

3rd step: Substitute eq 2.29 to 2.30

$$C_L = \sqrt{\frac{C_{D_o}\pi A R e}{3}} \quad (2.31)$$

4th step: Substitute eq 2.31 to 2.18

$$C_D = \frac{4C_{D_o}}{3} \quad (2.32)$$

5th(FINAL) step: Substitute equation 2.31 and 2.32 to C_L/C_D^2

$$\left(\frac{C_L}{C_D^2}\right)_{MAX} = \frac{3\sqrt{3}}{16} \sqrt{\frac{\pi A R e}{C_{D_o}^3}} \quad (2.33)$$

We end this subject by remarking that, especially, the maximum lift-to-drag ratio $(C_L/C_D)_{max}$, is a significant aerodynamic quantity of an aircraft (Ruijgrok, 2009).

2.3 Airfield Performance

A maneuver movement can be determined in the takeoff phase during the aircraft accelerated from rest on the runway with $v=0$ condition to climb out velocity v_c . Two main phases of takeoff distance are:

- The ground run distance
- Airborne distance

The takeoff distance consists of some phases, starting from pre-rotation phase from rest $v=0$ until rotation speed v_R , continuing with rotation phases from rotation speed v_R until liftoff speed v_{LOF} . v_R is a very influential factor during the takeoff path because in this phase, a pilot will decide to set up the upward aircraft rotation. And the overall takeoff maneuver safety can be affected and specified from this reference speed since there is a lot of shifting rotation speed v_R . During the initial segment of the ground run, the aircraft rate remains genuinely unaltered. Past the rotation speed, the angle of attack starts expanding from the ground stage toward the liftoff condition. And the airborne phase starts when the lift force is

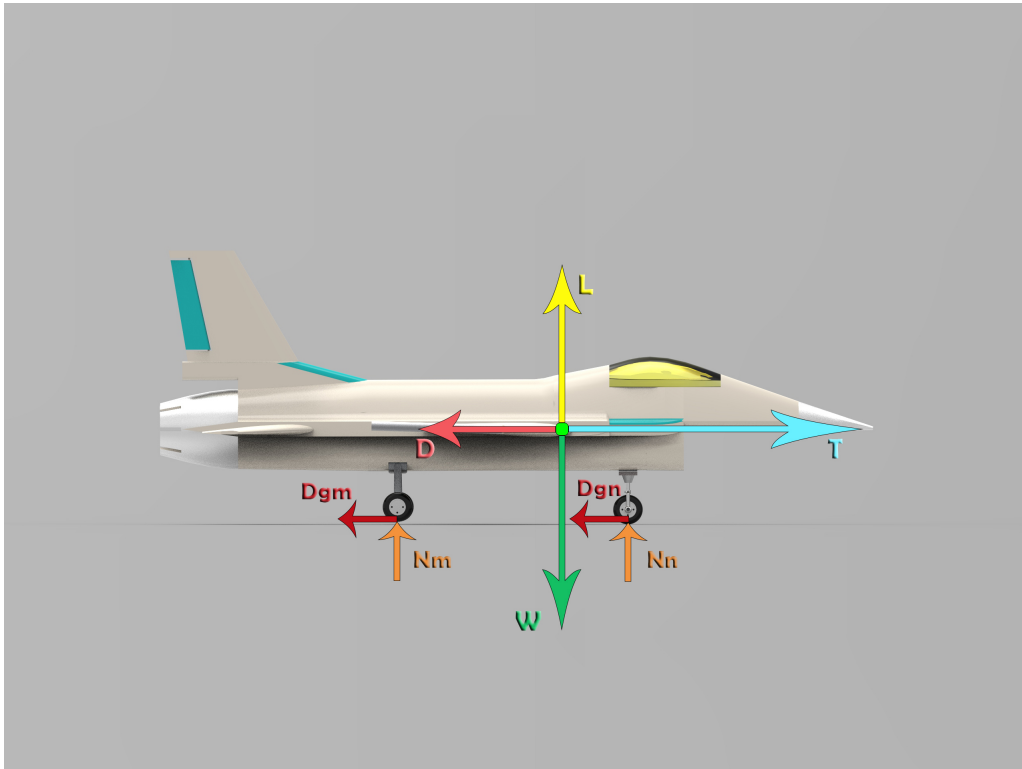


FIGURE 2.2: Force acting on UAV

equal to the aircraft weight. The airborne distance is normally isolated into the transition phase to climbing flight and the rectilinear climb to the screen height. In the transition stage, the flight path angle is raised from zero liftoff speed to the steady climb phase at screen velocity v_c , is flown with a steady lift coefficient to give enough lift force to achieve an adequate shape of the flight path. The flap deflection and engine control setting stay steady during the takeoff maneuver. Notwithstanding, to improve climb performance, the landing gear is withdrawn not long after the aircraft has gotten airborne. After passing through the screen, the aircraft goes along the takeoff flight path until it gets hold of at a protected flight condition at an altitude of around 450 m (1500 ft) where the proceeded climb to cruising elevation starts. (J. D. Anderson, 2015)

In the airworthiness requirements, during takeoff ground run, a multi engine aircraft must have to wait until there is no machine failure in certain range and speed. This is done so that safety in flight is maintained. no passenger felt threatened. To fulfill it, a pilot must watch the speed indicator in every takeoff phase,

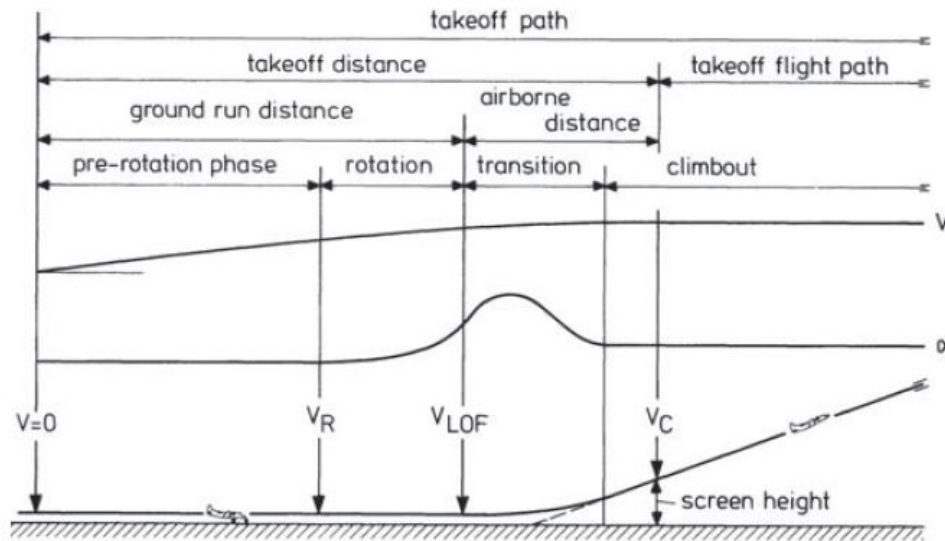


FIGURE 2.3: Take off maneuver (Ruijgrok, 2009)

Figure 2.4 explains about the order.

2.3.1 Take off ground run

Figure 2.2 shows all forces acting on an aircraft's ground run. The aircraft's weight is balanced by the lift force and wheel's normal force from the ground. And the Thrust is countered by drag and wheel's friction.

The frictional force from the wheels is:

$$\begin{aligned}
 Dg &= D_{gm} + D_{gn} \\
 &= \mu(N_m + N_n) \\
 &= \mu(W - L) \\
 &= \mu\left(W - \frac{1}{2}\rho v^2 S C_{Lg}\right)
 \end{aligned} \tag{2.34}$$

C_{Lg} = Lift Coefficient in the ground run attitude. μ = Rolling Friction Coefficient Where, for concrete ground and the asphalted runway, $\mu = 0.02$ and for a short cut grass, $\mu = 0.05$

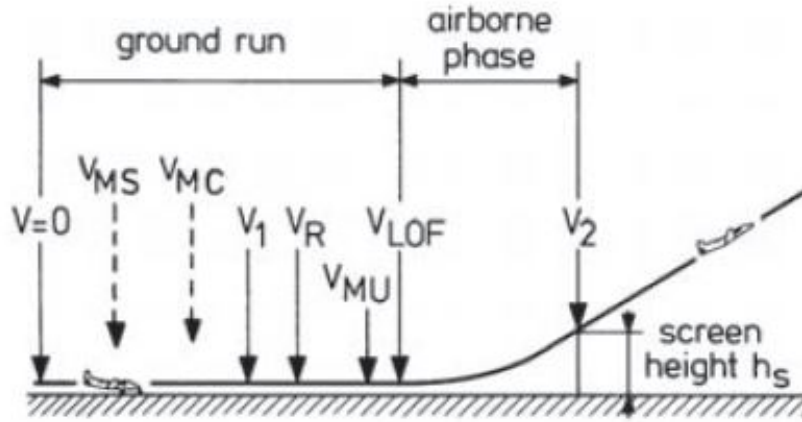


FIGURE 2.4: Takeoff reference speeds for conventional transports(Ruijgrok, 2009)

By neglecting the wind and runway does not have any slope, the motion's equation could be determined, such as: (Torenbeek, 2010)

$$\begin{aligned}
 F &= T - D - D_g \\
 &= T - \left[\frac{1}{2} \rho v^2 S \left(C_{D_o} + \Phi \frac{C_L^2}{\pi A R e} \right) \right] - D_g
 \end{aligned} \tag{2.35}$$

Φ = Ground effect for some explanation. This phenomenon is the cause of an airplane's tendency to float above the ground near the moment of landing. In the presence of a ground effect, the decreased drag is accounted for by Φ . Where,

$$\Phi = \frac{(16h/b)^2}{1 + (16h/b)^2} \tag{2.36}$$

During the ground run rotation phase, the C_{L_g} and C_{D_g} will vary. To get the aircraft acceleration during the ground run, indicate that $a = dv/dt$ and $v = ds/dt$, the distance accelerating from rest ($s=0, t=0$) to liftoff speed ($s=S_g, t=t$) can

PERFORMANCE REVIEW AND ANALYSIS OF GUAV-190417 TARGET DRONE:
AIRFIELDS, SYMMETRIC CLIMB, AND GLIDING

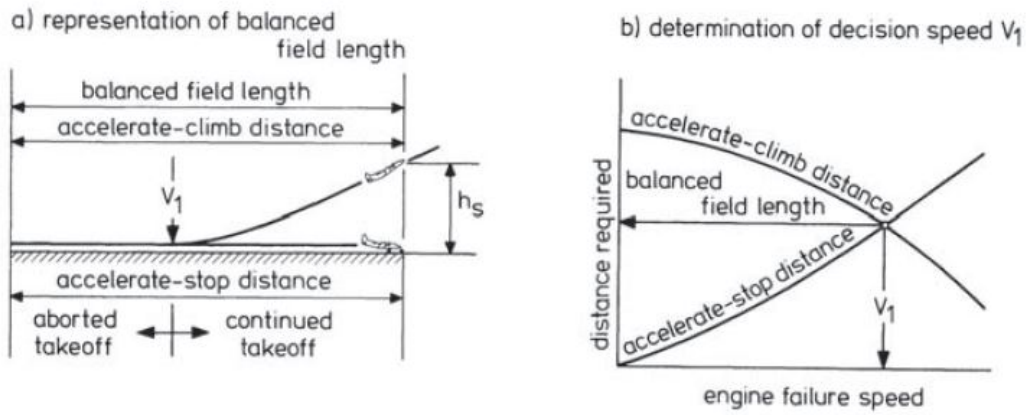


FIGURE 2.5: Balanced field length concept (Ruijgrok, 2009)

be written as:

$$\begin{aligned}
 a &= \frac{dv}{dt} \\
 a dt &= dv \\
 \int_0^t a dt &= \int_0^v dv \\
 at &= v \\
 t &= \frac{v}{a} \\
 t &= \frac{v}{\left(\frac{F}{m}\right)} \\
 t &= \frac{vm}{F}
 \end{aligned} \tag{2.37}$$

or,

$$v = \frac{F}{m}t \tag{2.38}$$

and for,

$$\begin{aligned}
 v &= \frac{ds}{dt} \\
 ds &= v dt \\
 \int_0^{S_g} ds &= \int_0^t v dt \\
 S_g &= \int_0^t v dt
 \end{aligned} \tag{2.39}$$

Substitute equation 2.38 and 2.39

$$\begin{aligned}
 S_g &= \int_0^t \frac{F}{m} t dt \\
 S_g &= \frac{F}{m} \frac{t^2}{2}
 \end{aligned} \tag{2.40}$$

Then, by substituting 2.37 to 2.40

$$\begin{aligned}
 S_g &= \frac{F}{m} \frac{t^2}{2} \\
 S_g &= \frac{F}{m} \frac{\left(\frac{vm}{F}\right)^2}{2} \\
 S_g &= \frac{F}{m} \frac{v^2 m^2}{2F^2} \\
 S_g &= \frac{v^2 m}{2F}
 \end{aligned} \tag{2.41}$$

Substitute equation 2.35 and 2.43 and also mass = W/g (J. D. Anderson, 1998)

$$S_g = \frac{v_{LOF}^2 W}{2g [T - D - \mu(W - \frac{1}{2}\rho v^2 SC_{L_g})]} \tag{2.42}$$

For take off safety, the takeoff speed (v_{LOF}) must be 20 percent higher than the stalling speed (V_{Stall}). So,

$$\begin{aligned}
 v_{LOF} &= 1.2v_{Stall} \\
 &= 1.2\sqrt{\frac{2W}{\rho SC_{L_{max}}}}
 \end{aligned} \tag{2.43}$$

Yield for the ground run distance (Ruijgrok, 2009)

$$\begin{aligned}
 S_g &= \frac{\left(1.2\sqrt{\frac{2W}{\rho SC_{L_{max}}}}\right)^2 W}{2g \left[T - D - \mu\left(W - \frac{1}{2}\rho v^2 SC_{L_g}\right)\right]} \\
 &= \frac{1.44\frac{2W^2}{\rho SC_{L_{max}}}}{2g \left[T - D - \mu\left(W - \frac{1}{2}\rho v^2 SC_{L_g}\right)\right]} \\
 &= \frac{1.44W^2}{g\rho SC_{L_{max}} \left[T - D - \mu\left(W - \frac{1}{2}\rho v^2 SC_{L_g}\right)\right]}
 \end{aligned} \tag{2.44}$$

2.3.2 The Airborne Phase of The Take Off

The airborne distance is heavily dependent on how the aircraft is operated by the pilot and can thus be measured only when two control laws are determined. The continuous engine control setting conditions during takeoff maneuvers decide one of them. The second control rule concern the lift coefficient time history, natural acceleration, or pitch rate from the moment the aircraft leaves the ground until at the end of the transfer, it enters a comfortable climbing attitude.

The exact specification of the flight path between the takeoff point and the screen's height is usually carried out by step-by-step calculations, following those control rules. (Francis J. Hale, 1984)

In a transition flare, Figure 2.6, the equation which can be written as

$$\frac{W}{g} v \frac{dv}{ds} = T \cos \alpha_T - D - W \sin \gamma \tag{2.45}$$

$$\frac{W}{g} \frac{v^2}{R} = L + T \sin \alpha_T - W \cos \gamma \tag{2.46}$$

If the thrust and velocity vector overlap ($\alpha_T = 0$) and the angle of the flight path is small ($\sin \gamma = \gamma$ and $\cos \gamma = 1$), the Figure governing motion equation is reduced to 2.7

$$\frac{W}{g} v \frac{dv}{ds} = T - D - W\gamma \tag{2.47}$$

$$\frac{W}{g} \frac{v^2}{R} = L - W \tag{2.48}$$

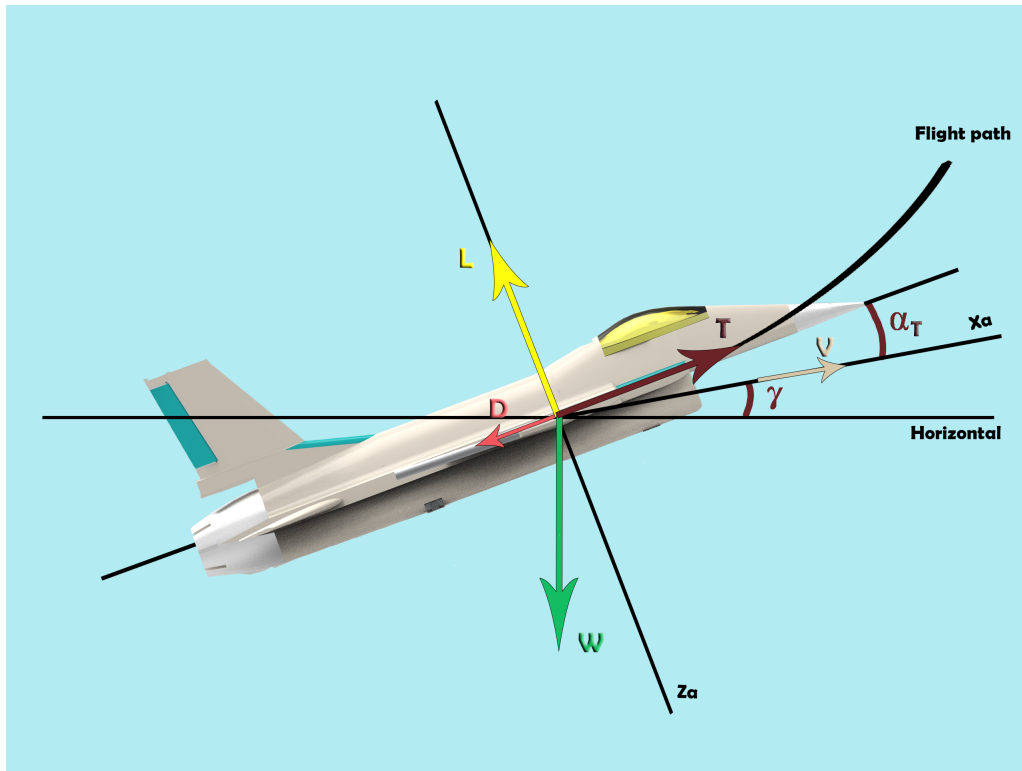


FIGURE 2.6: Equilibrium of forces during transition

A basic analytical solution to the issue is rendered here, considering a circular path of radius R. Thus, if the pilot automatically raises the angle at the take-off stage, we must consider shifting. Angle of attack and increase lift, move along the curve path Figure 2.8 section a.

The lift shifting coefficient, C_{Lt} , can be presented immediately after lift off as:

$$(C_{Lt})_{LOF} = (C_L)_{LOF} + \Delta(C_L)_{LOF} \quad (2.49)$$

At any stage on the next transition flight path, the lift coefficient could be written as Figure 2.8 section b.

$$C_{Lt} = (C_L)_{LOF} + \Delta C_L \quad (2.50)$$

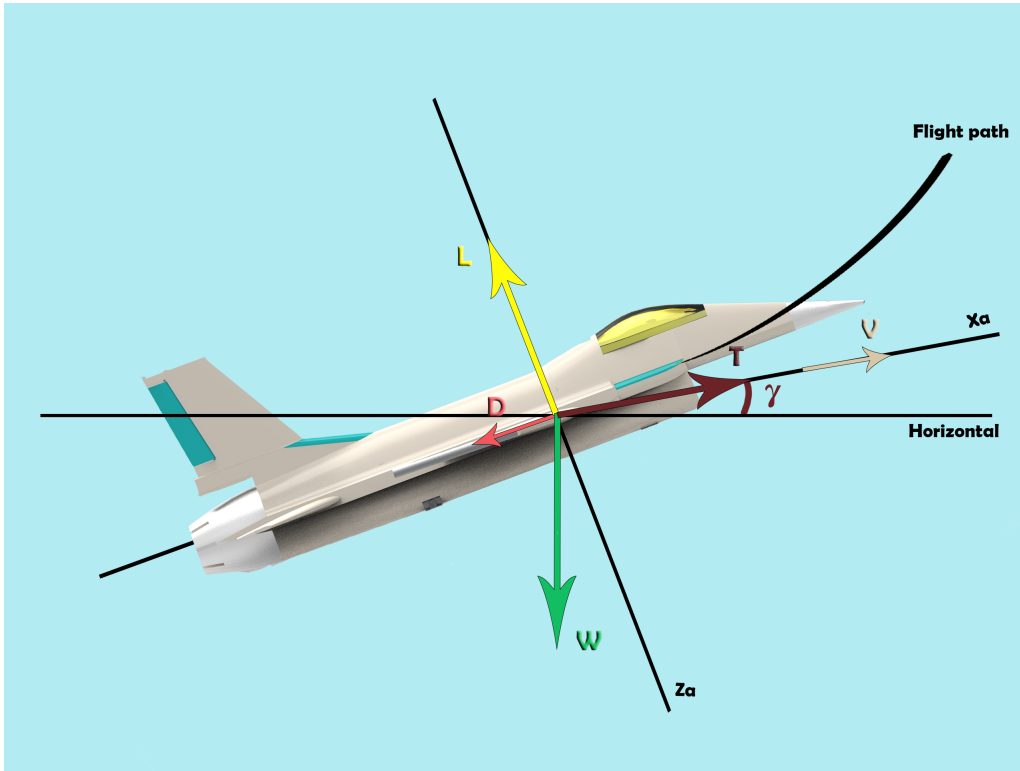


FIGURE 2.7: Equilibrium of forces during transition(2)

By substituting equation 2.50 into 2.48, the equation become:

$$\frac{1}{gR} = \frac{1}{v_{LOF}^2} - \frac{1}{v^2} + \frac{\Delta C_L}{\frac{2}{\rho} \frac{W}{S}} \quad (2.51)$$

This term illustrates that ΔC_L and C_{Lt} quantities during displacement would decline over time Figure 2.8 section b. We can express the radius R by the combination of equations 2.48 and 2.49

$$\begin{aligned} R &= \frac{2 \frac{W}{S}}{\rho g \Delta(C_L)_{LOF}} \\ &= \frac{v_{LOF}^2 (C_L)_{LOF}}{g \Delta(C_L)_{LOF}} \\ &= \frac{V_{LOF}^2}{g(n_{LOF} - 1)} \end{aligned} \quad (2.52)$$

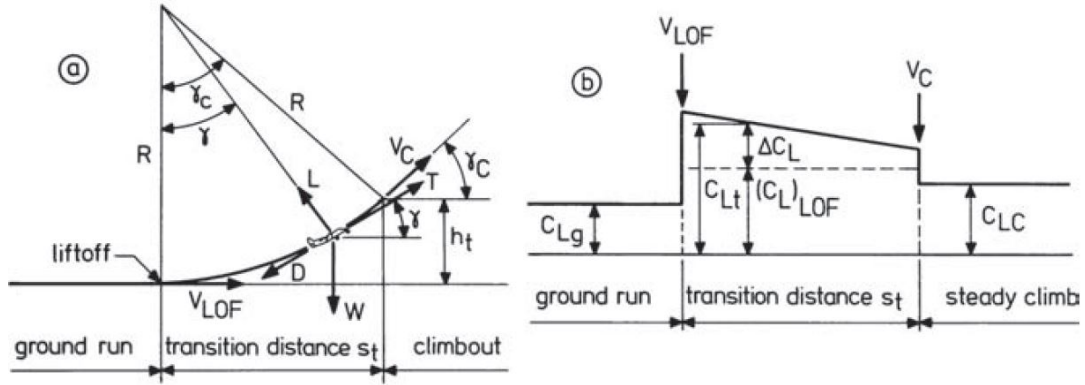


FIGURE 2.8: Schematic for transition to steady climb (Ruijgrok, 2009)

Where n_{LOF} is the load factor of lift off, (Raymer, 1989)

$$n = \frac{L}{W} = \frac{\frac{1}{2}\rho S(0.9C_{Lmax}(1.15v_{stall})^2)}{W} \quad (2.53)$$

Flight-path angle reaches the value,

$$\sin \gamma_c = \left(\frac{T - D}{W} \right) \quad (2.54)$$

The transition is done, and the steady climb starts at v_c airspeed. The sporadic value of the shifting coefficient at that stage in the flight path is unexpectedly reduced to the C_{Lc} value concerning the v_c velocity's stability.

$$C_{Lc} = \frac{W}{\frac{1}{2}\rho S v_c^2} \quad (2.55)$$

This is conveniently obtained from geometric patterns if R and C are known. The following relationship occurs in Figure 2.8 section a:

$$S_t = R \sin \gamma_c \quad (2.56)$$

$$h_t = R(1 - \cos \gamma_c) \quad (2.57)$$

2.3.3 Landing Ground Run

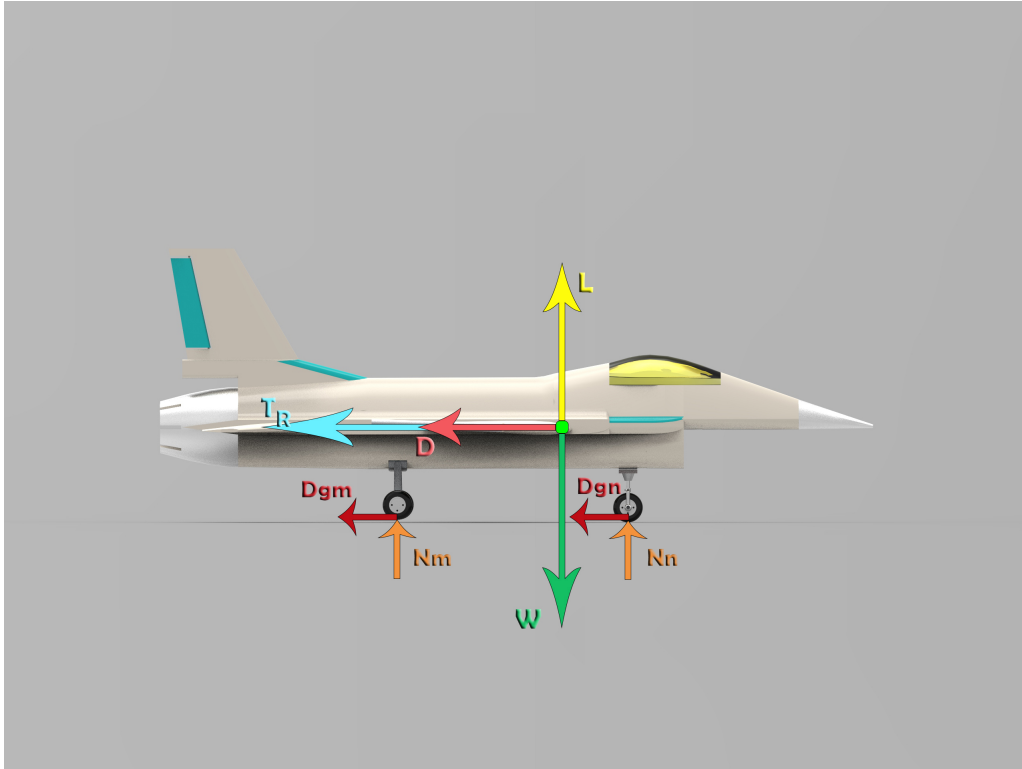


FIGURE 2.9: Force acting on UAV during landing

Figure 2.9 shows all forces acting on an aircraft's ground run. Due to the landing performance, the motion's equation doesn't change too much. As we know that the jet engines create a thrust reversal, the thrust goes in the same direction with drag force and the wheels' friction force. The equation is shown as:

$$\begin{aligned} F &= -T - D - D_g \\ &= -T - \left[\frac{1}{2} \rho v^2 S \left(C_{D_o} + \Phi \frac{C_L^2}{\pi A R e} \right) \right] - D_g \end{aligned} \quad (2.58)$$

The distance itself will also have different parameters, the distance accelerating condition is from landing speed ($s=S_L, t=0$) to rest ($s=0, t=t$). So,

$$\begin{aligned}
 v &= \frac{ds}{dt} \\
 ds &= v dt \\
 \int_{S_L}^0 ds &= \int_0^t v dt \\
 -S_L &= \int_0^t v dt \\
 -S_L &= \frac{v_T^2 m}{2F} \\
 -S_L &= \frac{v_T^2 W}{2g [-T - D - \mu(W - \frac{1}{2}\rho v^2 SC_{L_g})]} \\
 S_L &= \frac{v_T^2 W}{2g [T + D + \mu(W - \frac{1}{2}\rho v^2 SC_{L_g})]}
 \end{aligned} \tag{2.59}$$

Where for safety factor V_T need extra 30 percent speed from v_{Stall} ,

$$\begin{aligned}
 v_T &= 1.3v_{Stall} \\
 &= 1.3\sqrt{\frac{2W}{\rho SC_{L_{max}}}}
 \end{aligned} \tag{2.60}$$

By having the same substitution steps, the landing distance is became:

$$S_L = \frac{1.69W^2}{g\rho SC_{L_{max}} [T + D + \mu(W - \frac{1}{2}\rho v^2 SC_{L_g})]} \tag{2.61}$$

Where $\mu = 0.4$ because the pilot is applying a brake system (J. D. Anderson, 1998).

2.4 Climbing Performance

2.4.1 Quasi-steady symmetric

At this stage, we have successfully addressed the point of performance issues. Path performance or integral performance values that are linked with the direction of

flight will be suppressed. There are three priority integral performance values in the climbing phase, such as:

- The time needed to climb
- The distance covered during climbing on X-axis
- The fuel used in the climbing phase

The wind effect is negligible under these conditions. The time rate of altitude transition is the aircraft's rate of climb, also equivalent to the vertical airspeed.

$$RC = \frac{dh}{dt} = v \sin \gamma \quad (2.62)$$

$$dt = \frac{dh}{RC} = \frac{dH}{RC} \quad (2.63)$$

Integration on equation 2.63 requires the time during the climb from altitude H_1 to H_2 .

$$t = \int_{H_1}^{H_2} \frac{dH}{RC} \quad (2.64)$$

Rate of Climb is a function affected by aircraft weight, airspeed, altitude, and engine control setting. Without being affected by wind, this equation is to determine the x-axis distance.

$$s = \int_{t_1}^{t_2} v \cos \gamma dt = \int_{H_1}^{H_2} \frac{dH}{\tan \gamma} \quad (2.65)$$

$$W_f = \int_{t_1}^{t_2} F dt = \int_{H_1}^{H_2} \frac{F}{RC} dH \quad (2.66)$$

This equation is used to determine the fuel used weight during the climbing phase. Fuel weight flow rate symbolized with 'F'.

To get a minimum time for climbing, we must maximize the rate of climb at the respective altitude.

$$t_{\min} = \int_0^H \frac{dH}{RC_{\max}} \quad (2.67)$$

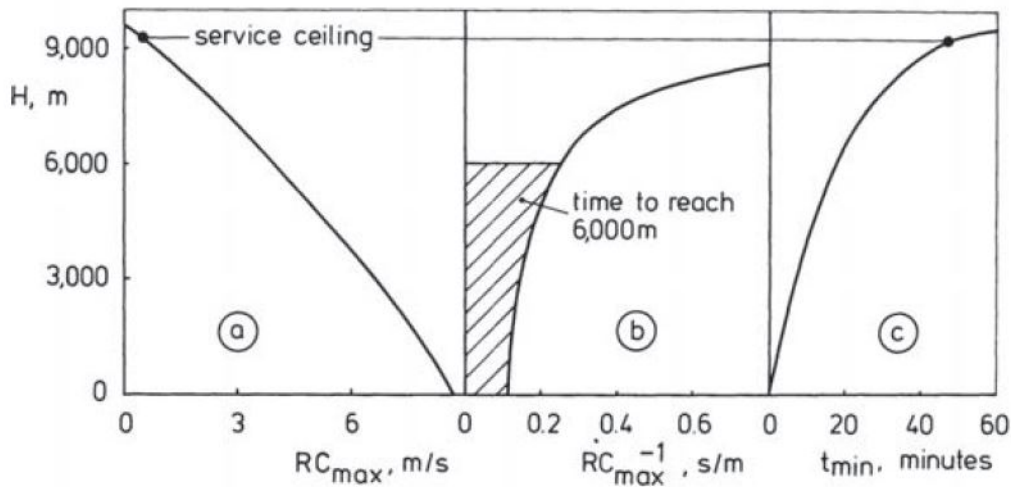


FIGURE 2.10: Characteristic of RC and Time Minimum due to Altitude(Ruijgrok, 2009)

Composing this equation can be determined by assuming the maximum rate of climb decreases straightly with an aircraft's height. RC_{max0} is Rate of Climb in sea level conditions and H_{th} for the theoretical ceiling condition height.

$$\frac{RC_{max}}{RC_{max0}} = \frac{H_{th} - H}{H_{th}} \quad (2.68)$$

Minimum time equation can be determine by integrating and substituting between equation 2.67 and Eq 2.68

$$t_{min} = \frac{H_{th}}{RC_{max}} \ln \left(\frac{1}{1 - \frac{H}{H_{th}}} \right) \quad (2.69)$$

The eq 2.67 integration can be achieved graphically from RC_{max} to H, and they don't have any analytic expressions. In Figure 2.10 section B, the minimum time during the climb phase can be determined by calculating the area of the curve left section, where the curve shows the y-axis for Altitude and x-axis for RC_{max}^{-1} . The C section outcome, figure out 47.5 min for the minimum time needed to reach 9250 meters service ceiling altitude.

Increments in time between altitude intervals can be applied to obtain the climb time required.

$$t = \sum_{i=1}^n \left[\frac{\Delta H}{RC_i} \right] \quad (2.70)$$

By varying the altitude above sea level, we will get the rate of climb in each altitude, this rate of climb which of course will determine the absolute and service ceilings altitude of the aircraft. The relationship between rate of climb and altitude is: :

- Absolute Ceilings Altitude is when the Rate of Climb is equal to 0.
- Service Ceilings Altitude is when the Rate of Climb is equal to 0.508 ms^{-1} .

The rho must be adjusted corresponding to the various altitude. The airspeed is determined where:

$$\begin{aligned} W &= L \\ W &= \frac{1}{2} \rho v^2 S C_L \\ v &= \sqrt{\frac{2W}{\rho S C_L}} \end{aligned} \quad (2.71)$$

During the rho difference, the thrust also get affected, where:

$$\frac{T}{T_0} = \left(\frac{\rho}{\rho_0} \right)^{0.75} \quad (2.72)$$

To determine the maximum Rate of Climb, the equation shown as:

$$\begin{aligned} RC_{\max} &= \frac{Pa}{W} - \sqrt{\frac{2W}{\rho S \left(\frac{C_L^3}{C_D^2} \right)_{\max}}} \\ RC_{\max} &= \frac{TV}{W} - \sqrt{\frac{2W}{\rho S \left(\frac{C_L^3}{C_D^2} \right)_{\max}}} \end{aligned} \quad (2.73)$$

Where RC_i is the average point of rate of climb between the certain height difference intervals.

From each height difference interval, the weight of fuel used can also be determined with this equation.

$$\Delta W_{fi} = F_i \Delta t_i \quad (2.74)$$

Where the fuel weight flow rate average is written with F_i . And in the adjacent interval of rate of climb at aircraft weight can be calculated as:

$$W_{i+1} = W_i - \Delta W_{fi} \quad (2.75)$$

And from those equations, we can calculate the total fuel used in the climb phase.

$$W_f = \Sigma \Delta W_{fi} \quad (2.76)$$

In conclusion, the drag is larger than the thrust because of the negative flight path angle. So we don't need to divide the development because the preceding general performance theory is already included in the descending flight formula. A constant engine control framework and constant Mach number timetable may be stated in Descent Program until they reach the particular velocity operation. Generally, timetable suggestions may have deliberation adjustment with the local air traffic control regulation (Ruijgrok, 2009).

2.5 Gliding Flight

Gliding is a flight condition when the aircraft's engine does not create any thrust. For example, the engineless glider, this type does not have any component to produce thrust, so it just glides until losing lift force. When an aircraft is flying in idle condition, the engines only produce a very small propulsive force, so we can assume there's no thrust acting during the gliding flight.

Figure 2.11 shows us, during the glide, an aircraft will create an angle between its body and x-axis. We called it gamma. Because there is no thrust in gliding condition, we can set T is equal to 0. So we can obtain this equation:

$$\begin{aligned} -D + W \sin \gamma &= 0 \\ D &= W \sin \gamma \end{aligned} \quad (2.77)$$

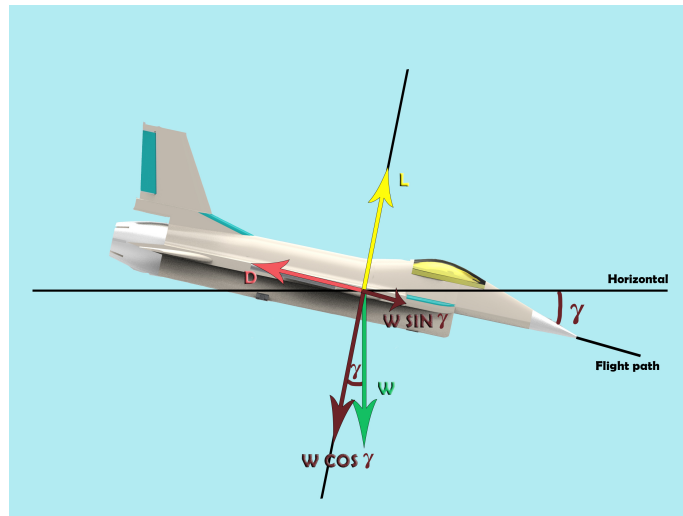


FIGURE 2.11: Force acting on Gliding Flight

$$L - W \cos \gamma = 0$$

$$L = W \cos \gamma \quad (2.78)$$

By substitute equation 2.77 and 2.78, we could find out the gamma:

$$W = W$$

$$\frac{D}{\sin \gamma} = \frac{L}{\cos \gamma}$$

$$\frac{\sin \gamma}{\cos \gamma} = \frac{D}{L}$$

$$\tan \gamma = \frac{\frac{1}{2} \rho v^2 S C_D}{\frac{1}{2} \rho v^2 S C_L} \quad (2.79)$$

$$\tan \gamma = \frac{C_D}{C_L}$$

$$\tan \gamma = \frac{1}{\frac{C_L}{C_D}}$$

To get a lower angle, ratio of C_L and C_D should be in maximal:

$$\tan \gamma = \frac{1}{\left(\frac{C_L}{C_D}\right)_{\max}} \quad (2.80)$$

And from equation 2.78. The airspeed formula can be shown as:

$$\begin{aligned}
 L &= W \cos \gamma \\
 \frac{1}{2} \rho v^2 S C_L &= W \cos \gamma \\
 v &= \sqrt{\frac{W}{S} \frac{2}{\rho} \frac{1}{C_L} \cos \gamma}
 \end{aligned} \tag{2.81}$$

The rate of descent also can figure out by substitute equation 2.81 with 2.80

$$\begin{aligned}
 RD &= v \sin \gamma \\
 &= v \frac{C_D}{C_L} \cos \gamma \\
 &= \sqrt{\frac{W}{S} \frac{2}{\rho} \frac{C_D^2}{C_L^3} \cos^3 \gamma}
 \end{aligned} \tag{2.82}$$

Those equations are valid when the aircraft acts on a low subsonic flight speed because at low subsonic condition. We are ignoring the Reynolds number effect. The angle of attack is the only one control variable to define V , γd , and RD .

During gliding, a pilot hopes to perform the farthest range and maximum length of time. These could be obtained if the aircraft can hold the minimum rate of descent. To get the maximum length of time, the equation should be integrated: (Ruijgrok, 2009)

$$\begin{aligned}
 t_{\max} &= \int_H^0 \frac{-dH}{RD_{\min}} \\
 &= \frac{H}{RD_{\min}}
 \end{aligned} \tag{2.83}$$

And for the longest/farthest range:

$$\begin{aligned}
 R_{\max} &= \frac{H}{\tan \gamma} \\
 &= H \left(\frac{C_L}{C_D} \right)_{\max}
 \end{aligned} \tag{2.84}$$

CHAPTER 3

RESEARCH METHODOLOGY

Overview

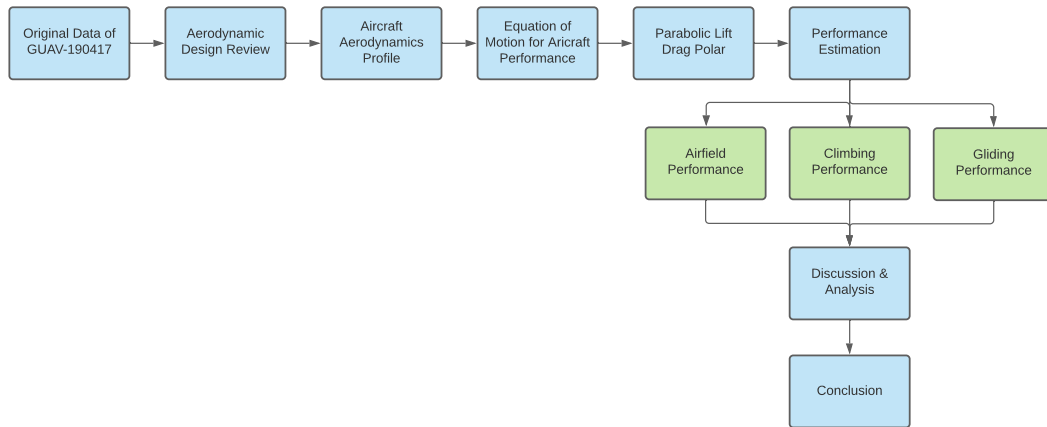


FIGURE 3.1: Major Step

In chapter 3, we will discuss the research flow that will be carried out in this thesis. In its flow which shown in Figure 3.1, eight phases in particular must be considered. The first phase was the processing of original data from the GUAV-190417 Target Drone. UAV wing dimensions, airfoil characteristics, and engine characteristics were included in the collection. Then, in the second step, GUAV design will be reviewed in aerodynamic parameters through open foam software. This step aims to compare the lift coefficient and drag coefficient in manual calculation with software calculations. In step 3, the calculation of the characteristic aircraft variable will be carried out. The calculated variables are the aspect ratio, Reynolds number, etc. The elaboration of the primary forces on the aircraft would be calculated in the fourth stage to measure the polar parabolic lift drag in the fifth step. The aircraft characteristics, such as lift-drag coefficient, drag force derivation, and maximum aerodynamic ratio, will be defined in this stage. The sixth stage

is a performance review, which is the conclusion of the topic of this thesis, where three performances, namely airfield performance, gliding performance and cruising efficiency, are to be analyzed. The implications of this study would be explored and concluded as plausible.

3.1 Original Data of GUAV-190417

The mission profile and the target drones design requirements were set by carrying out a benchmark study from the conceptual design phase. The mean values from the benchmark study were used as a reference to pick out different configurations that would be short-listed depending on the design factor. The chosen configuration defines the body type, wing type, wing position, engine position, canard, tail, fuel tank and capacity, braking system, and landing gear to determine the target drones shape. The type of airfoil, material, engine, electrical components, and payload was also selected.

Using the data obtained from the benchmark study, the preliminary sizing for the target drone can be determined. Once finalized, a draft design is assembled by utilizing solid edge as the project's CAD software. By choosing the target drone material, solid edge allows users to estimate the weight, center of gravity, and aerodynamic center of the target drone. The specifications and characteristics of the engine and airfoil were already available.

Variables given by GUAV-190417:

- Aircraft body:
 - Length
 - Wingspan
 - Swept angle
 - Area
 - Estimation Total Weight
- Engine specification:
 - Thrust maximum

- Mass fuel rate
- Mach number

3.2 Aerodynamic Design Review

In the aerodynamic design review, OpenFOAM v8.0 software was used to simulate the viscous pressure of the GUAV-190417 design to determine the aerodynamics characteristics, i.e., lift and drag coefficients. The laminar simulation was carried out using a steady-state scheme using simpleFOAM solver. The model whose size 0.4 times of actual one was constructed using CAD software Solid Edge and then imported to pre-processing functions in OpenFOAM. The computational length, height, and width of the computational domain are 1.7, 1, and 0.5, in x , y , and z directions, respectively, in non-dimensional values. Note that only half of the flow around the aircraft was simulated to reduce computational time since the aircraft is symmetric in $x - y$ plane. It is also worth mentioning that the aircraft's front nozzle was defined as a closed structure and a slight increase in pressure drag was expected.

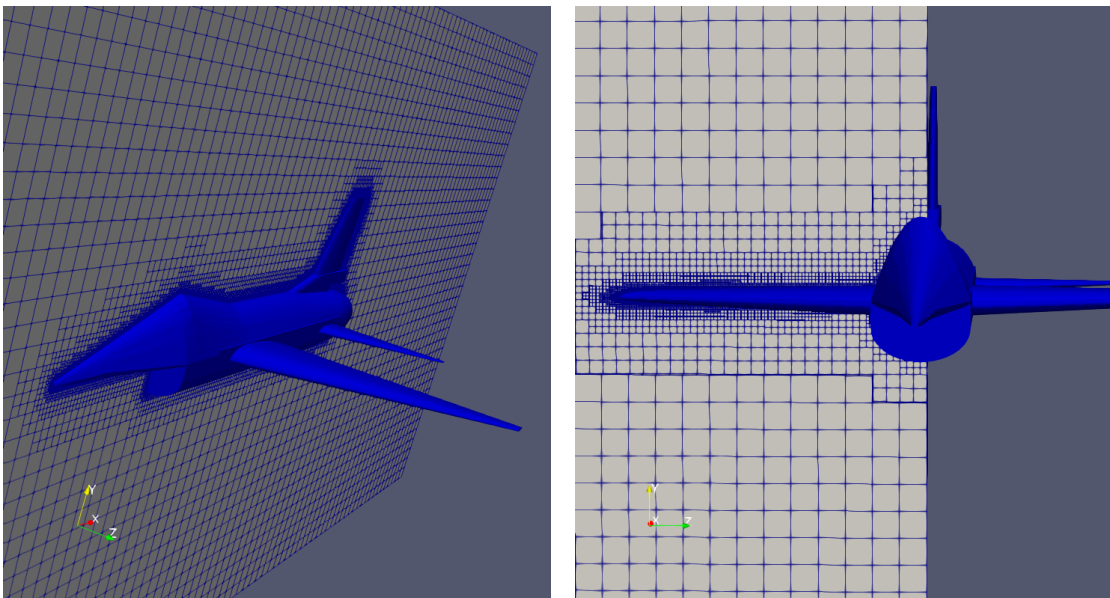


FIGURE 3.2: Mesh topology of computational domain

The mesh generator used to discretize the computational domain is snappy-HexMesh (see OpenFOAM User Guide (OpenFoam, 2012) to construct this mesh). This simulation's total meshes are 4517622 elements, consisting of 3647081 hexahedral elements, 195682 prism elements, and 674859 polyhedral elements. The boundary condition's streamwise velocity was set to 100 in non-dimensional value. In contrast, other component velocities (such as transverse and spanwise velocities) were set to zero to represent the flow in zero angles of attack ($\alpha = 0$). The aircraft model was defined as no-slip wall boundary condition, such that $\frac{d\phi}{dn} \neq 0$. The total computational time of 5000 iterations is ~ 26 hours using 4 processors and 16 GB RAM, where the convergence was reached after 2000 iteration. The results were analyzed using Paraview software. The Figure 3.2 shows the output of the meshing.

Apart from using software, manual calculations are also carried out, For lift coefficient, the formula applied as,

$$C_L = \frac{L}{\frac{1}{2}\rho v^2 S} \quad (3.1)$$

and for drag coefficient, the formula applied as,

$$C_D = \frac{D}{\frac{1}{2}\rho v^2 S} \quad (3.2)$$

Where the velocity is applied at 100m/s and 0.0768 for the scale model area. The lift and drag coefficient values that are looking for here are the overall values of the whole aircraft, starting from the fuselage, wing, horizontal stabilizer and vertical stabilizer. Where,

$$C_{Do} = C_{Dowing} + C_{Dofuselage} + C_{D Kempennage} + C_{Doothers} \quad (3.3)$$

3.3 Aircraft Aerodynamics Profile

Aircraft aerodynamics profile can be obtained by calculating variables provided by the airfoil characteristic and wing dimension tables (original data of GUAV-190417)

in Chapter 1. Those variables generate: (Sadraey, 2012)

$$AR = \frac{b^2}{S} \quad (3.4)$$

$$e = 4.61(1 - 0.045AR^{0.68})[\cos(\Lambda_{LE})]^{0.15} - 3.1 \quad (3.5)$$

$$k = \frac{1}{\pi A Re} \quad (3.6)$$

$$Re = \frac{\rho v S}{\text{Viscosity}} \quad (3.7)$$

$$\text{Taper Ratio} = \frac{C_t}{C_r} \quad (3.8)$$

3.4 Parabolic Lift Drag Polar

Aircraft Characteristic includes force coefficients such as the lift coefficient and drag coefficient. To get C_L and C_D , we declare that the aircraft is in equilibrium condition without the angle of attack works on it ($\alpha = 0$) and is located on the ground with zero altitudes above sea level ($H = 0$). This situation creates the lift and drag have an equal value, how. However, the drag and thrust also have the same value. This situation creates that:

- Lift and weight have an equal value. And,

$$\begin{aligned} L &= W \\ \frac{1}{2}\rho v^2 S C_L &= W \\ C_L &= \frac{2W}{\rho v^2 S} \end{aligned} \quad (3.9)$$

- Drag and thrust have an equal value.

$$\begin{aligned}
 D &= T \\
 \frac{1}{2}\rho v^2 S C_D &= T \\
 C_D &= \frac{2T}{\rho v^2 S}
 \end{aligned} \tag{3.10}$$

Then from those equations, we could get C_L and C_D .

Drag coefficient divides into zero-lift drag coefficient and induced drag coefficient.

$$C_D = C_{D_o} + C_{D_i} \tag{3.11}$$

Because the induced drag coefficient is impacted by the lift coefficient, we may get the C_{D_i} value from

$$C_{D_i} = \frac{C_L^2}{\pi A R e} \tag{3.12}$$

And for the zero-lift drag coefficient, we need to eliminate it by the equation:

$$C_{D_o} = C_D - C_{D_i} \tag{3.13}$$

The lift coefficient, drag coefficient, and zero drag coefficient are used for the next discussions. Especially in the maximum aerodynamics ratio, such as C_L/C_D , C_L^3/C_D^2 and C_L/C_D^2 . We can see the derivative of the maximum aerodynamics ratio in chapter 2.

$$\left(\frac{C_L}{C_D}\right)_{\max} = \frac{1}{2}\sqrt{\frac{\pi A R e}{C_{D_o}}} \tag{3.14}$$

$$\left(\frac{C_L^3}{C_D^2}\right)_{\max} = \frac{3\sqrt{3}}{16}\pi A R e\sqrt{\frac{\pi A R e}{C_{D_o}}} \tag{3.15}$$

$$\left(\frac{C_L}{C_D^2}\right)_{\max} = \frac{3\sqrt{3}}{16}\sqrt{\frac{\pi A R e}{C_{D_o}^3}} \tag{3.16}$$

3.5 Airfield Performance

3.5.1 Take Off Ground Run

Several factors need to be considered to determine the Take-off ground run, such as eq:

$$S_g = \frac{v_{LOF}^2 m}{2F} \quad (3.17)$$

Where,

- Mass

The mass can be determined by dividing the total weight by gravitation.

$$m = \frac{W}{g} \quad (3.18)$$

- Speed during take-off

For take-off safety, the take-off speed (VLOF) must be 20 percent higher than the stalling speed (VStall). To determine Vstall, we use CLmax, where CLmax can be calculated with equation:

$$C_{L\alpha} = \frac{C_{l\alpha}}{1 + \frac{C_{l\alpha}}{\Pi AR}} \quad (3.19)$$

$$C_{Lmax} = C_{L\alpha} \alpha_{max} \quad (3.20)$$

$$v_{LOF} = 1.2 \sqrt{\frac{2W}{\rho S C_{Lmax}}} \quad (3.21)$$

- Force The force consists of:

- Thrust force

The engine produces the thrust, and the value has been given in the chapter 1 table Aircraft Characteristic

- Drag force

Drag force can be determined by summing the Zero lift drag force and

Induced drag force, where the induced drag will have an additional multiplication by the ground effect factor.

$$D = \frac{1}{2}\rho v^2 S \left(C_{D_o} + \Phi \frac{C_L^2}{\pi A Re} \right) \quad (3.22)$$

where,

$$\Phi = \frac{(16h/b)^2}{1 + (16h/b)^2} \quad (3.23)$$

– Wheel friction force

The force could be determined by multiplying the friction coefficient with the Normal force of the aircraft. Where the normal is equal to Weight - Lift.

$$Dg = \mu(W - \frac{1}{2}\rho v^2 S C_{L_{max}}) \quad (3.24)$$

So to determine the Take Off Ground Run Distance, we use:

$$S_g = \frac{1.44W^2}{g\rho S C_{L_{max}} [T - D - \mu(W - \frac{1}{2}\rho v^2 S C_{L_g})]} \quad (3.25)$$

3.5.2 The Airborne Phase of The Take Off

To determine the airborne performance, an airplane needs the same radius value from the liftoff to the climb phase and the flight path's angle. To determine it, we use the formula:

$$R = \frac{v_{LOF}^2}{g(n_{LOF} - 1)} \quad (3.26)$$

Where, n_{LOF} is the load factor at liftoff.

$$n = \frac{\frac{1}{2}\rho S (0.9 C_{L_{max}} (1.15 v_{stall})^2)}{W} \quad (3.27)$$

Flight-path angle reaches the value,

$$\sin \gamma_c = \left(\frac{T - D}{W} \right) \quad (3.28)$$

This is conveniently obtained from geometric patterns if R and C are known. We can obtain the transition range distance in x-axis and transition altitude distance in y-axis, the formula shown as:

$$S_t = R \sin \gamma_c \quad (3.29)$$

$$h_t = R(1 - \cos \gamma_c) \quad (3.30)$$

3.5.3 Landing Ground Run

Meanwhile, to determine the landing ground run. We still apply total weight without fuel weight loss. To determine the landing ground run, several factors need to be considered, such as:

$$S_g = \frac{v_T^2 m}{2F} \quad (3.31)$$

Where,

- Mass

The mass can be determined by dividing the total weight by gravitation.

$$m = \frac{W}{g} \quad (3.32)$$

- Landing speed

Same as when take-off, during the landing, there is also a landing safety factor, where the landing speed (V_T) must be 30 percent higher than the stalling speed (V_{Stall}).

$$C_{L\alpha} = \frac{C_{l\alpha}}{1 + \frac{C_{l\alpha}}{\Pi AR}} \quad (3.33)$$

$$C_{L_{\max}} = C_{L\alpha} \alpha_{\max} \quad (3.34)$$

$$v_T = 1.3 \sqrt{\frac{2W}{\rho S C_{L_{\max}}}} \quad (3.35)$$

- Force

There is a difference in the force that applies because Reverse thrust is installed. The direction of reverse thrust becomes the same as the wheel friction force and drag force. Likewise, the friction coefficient has become 0.4 because of the braking system that works. Therefore the force value becomes larger.

$$F = -T - D - D_g \quad (3.36)$$

So to determine the Landing Ground Run Distance, we use:

$$S_L = \frac{1.69W^2}{g\rho SC_{L_{\max}} \left[T + D + \mu(W - \frac{1}{2}\rho v^2 SC_{L_{\max}}) \right]} \quad (3.37)$$

3.6 Climbing Performance

In this section, there are three priority integral performance values in the climbing phase to be determined, such as:

- The time needed to climb
- The fuel used in the climbing phase
- The distance covered during climbing on X-axis

To determine these 3 values, the first step that we must to assume the altitude condition. Remember that the air density in several altitudes has a different value. So before calculating the Rate of Climb, we must convert the air density by referencing the ISA characteristic as in Figure 3.3 due to several altitudes. We can use the equation:

For Temperature in gradient condition,

$$\ln \left(\frac{P_1}{P_0} \right) = -\frac{g}{R\lambda} \ln \left(\frac{T_1 + \lambda(H_1 - H_0)}{R} \right) \quad (3.38)$$

PERFORMANCE REVIEW AND ANALYSIS OF GUAV-190417 TARGET DRONE:
AIRFIELDS, SYMMETRIC CLIMB, AND GLIDING

The *Standard Atmosphere* temperature profile can be described using the following graph, divided into *isothermal* and *gradient* regions:

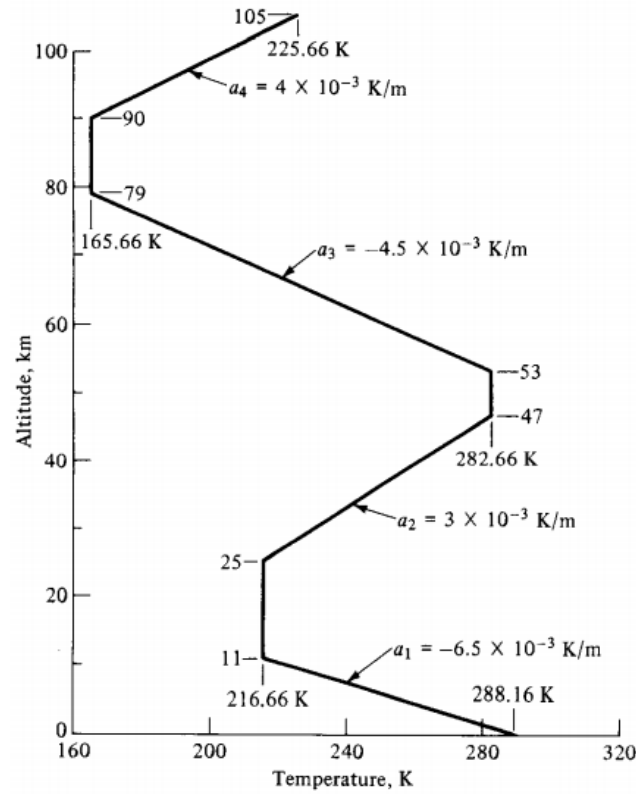


FIGURE 3.3: ISA Graph

For Temperature in constant condition,

$$\ln\left(\frac{P_1}{P_0}\right) = -\frac{g}{R\lambda} \ln\left(\frac{T_1 + \lambda(H_1 - H_0)}{R}\right) - \frac{g}{R(T_1)}(H_2 - H_1) \quad (3.39)$$

Then the density will be get by using gas constant ratio comparison.

$$\rho_1 = \frac{P_1 T_0}{P_0 T_1} \rho_0 \quad (3.40)$$

The difference rho also impacts Velocity and Thrust because of that to convert, we use For V:

$$v = \sqrt{\frac{2W}{\rho S C_L}} \quad (3.41)$$

For Thrust at Altitude less than 11,000 meter:

$$T_1 = \left(\frac{\rho_1}{\rho_0} \right)^{0.75} T_0 \quad (3.42)$$

For Thrust at Altitude more than 11,000 meter:

$$T_1 = \frac{\rho_1}{\rho_0} T_0 \quad (3.43)$$

With those values of thrust and airspeed, we can multiply them and get the Power available, which will then be used to find Climb's Maximum Rate. The equation:

$$RC_{\max} = \frac{Pa}{W} - \sqrt{\frac{W}{S} \frac{2}{\rho} \frac{1}{\left(\frac{C_L^3}{C_D^2} \right)_{\max}}} \quad (3.44)$$

The RC_i is the average Maximum Rate of Climb at the altitudes of H1 and H2.

$$RC_i = \frac{RC_{\max 0} + RC_{\max 1}}{2} \quad (3.45)$$

By having the RC_i, we can calculate the time difference between the height of H1 and H2. The equation is written as:

$$\Delta t_i = \frac{H_1}{RC_i} \quad (3.46)$$

For the time needed to climb itself, it can be found by:

$$t_1 = t_0 + \Delta t_i \quad (3.47)$$

To determine the change of Fuel Used,

$$\Delta W_{fi} = (mf)\Delta T_i g \quad (3.48)$$

Total fuel used:

$$W_{f1} = W_{f0} + \Delta W_{fi} \quad (3.49)$$

The amount of distance covered during climbing on X-axis could be determined by,

$$s = \frac{H_2 - H_1}{\tan \gamma} \quad (3.50)$$

Where,

$$\gamma = \sin^{-1} \frac{v}{RC} \quad (3.51)$$

3.7 Gliding Performance

Fortunately for gliding performance, the maximum altitude achieved through the calculation of Climbing Performance. With this attitude, we use the appropriate air density characteristics.

The first stage is to assume and vary the lift coefficient. Then the drag coefficient can be obtained by adding the zero-lift drag coefficient and the induced drag resulting from the effect of the lift.

$$C_D = C_{D_o} + \frac{C_L^2}{\pi A Re} \quad (3.52)$$

Next, what needs to be calculated is the ratio between C_L/C_D , C_L^3/C_D^2 .

If all the variables above have been found, we can find the descent degree of the plane with the formula:

$$\gamma_d = \tan^{-1} \left(\frac{1}{C_L/C_D} \right) \quad (3.53)$$

For the velocity, the equation is shown as:

$$v = \sqrt{\frac{2W \cos(\gamma_d)}{\rho S C_L}} \quad (3.54)$$

The rate of descent calculation is obtained by multiplying v by the sine of the descent degree that we obtained earlier.

$$RD = v \sin(\gamma_d) \quad (3.55)$$

And for horizontal velocity, just multiply v by the cosine of the descent degree,

$$v_h = v \cos(\gamma_d) \quad (3.56)$$

To get the maximum length of time, the equation should be integrated:

$$\begin{aligned} t_{\max} &= \int_H^0 \frac{-dH}{RD_{\min}} \\ &= \frac{H}{RD_{\min}} \end{aligned} \quad (3.57)$$

And for the longest/farthest range:

$$\begin{aligned} R_{\max} &= \frac{H}{\tan \gamma} \\ &= H \left(\frac{C_L}{C_D} \right)_{\max} \end{aligned} \quad (3.58)$$

CHAPTER 4

RESULTS AND DISCUSSIONS

4.1 Aircraft Characteristic

In UAV's performance analysis, the aircraft's characteristics are needed to determine the forces that affect an aircraft. Table 4.1 shows the variable that will use to determine the characteristic of aircraft, this calculation followed the formula in Chapter 2, which depends on wing dimension. (Sadraey, 2012)

TABLE 4.1: Wing Characteristic

| Variable | Value |
|-------------|------------------|
| AR | 7.627 |
| e | 0.646 64 |
| k | 0.064 54 |
| Re | 11×10^6 |
| Taper Ratio | 0.102 16 |

Corresponding to the Table 4.1, those variable is used for the aircraft aerodynamics profile calculation. Table 4.2 shows the result of the lift and drag coefficient. And by differentiating the drag force acting on the aircraft, we would get the parabolic lift drag polar variables, and also including the maximum aerodynamics ratio.

4.2 Aerodynamic Design Review

Figure 4.1 provides an overview of the contour results pressure, which only evaluated at the wall. The pressure values of the whole aircraft are drawn by mirroring

TABLE 4.2: Wing Characteristic(2)

| Variable | Value |
|------------------------|----------|
| C_{Do} | 0.0467 |
| $(C_L/C_D)_{\max}$ | 9.6035 |
| $(C_L^3/C_D^2)_{\max}$ | 96.6466 |
| $(C_L/C_D^2)_{\max}$ | 148.5153 |

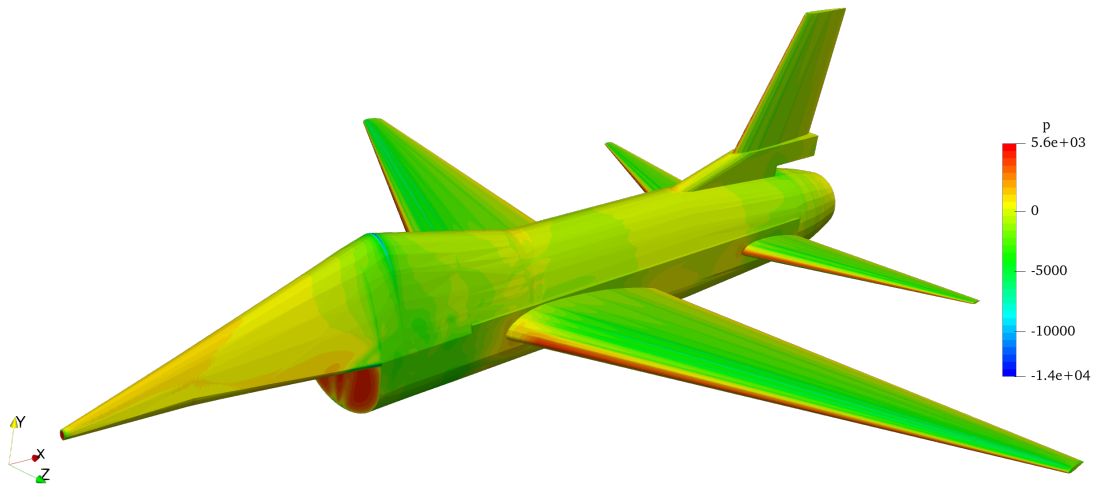


FIGURE 4.1: The pressure contour.

the half result. The red color represents the highest pressure level, followed by yellow, green, and blue, where the blue shows the lowest pressure level. And as in Figure 4.1, the color indication under the wing is yellow and red, while on the upper wing, the color is green. In conclusion, the lower part of the wing has greater pressure than the top of the wing.

The assumption of laminar, half computation model and $\frac{1}{2.5}$ scale model with reference area 0.0768 are applied in the simulation. The lift coefficient from the simulation shows almost the same results as the manual calculation. The lift coefficient using OpenFOAM is 0.3826, while in manual calculations using the $C_{L\alpha}$ chart, the value is 0.3529.

In calculating the manual zero lift drag polar coefficient, the value cannot be

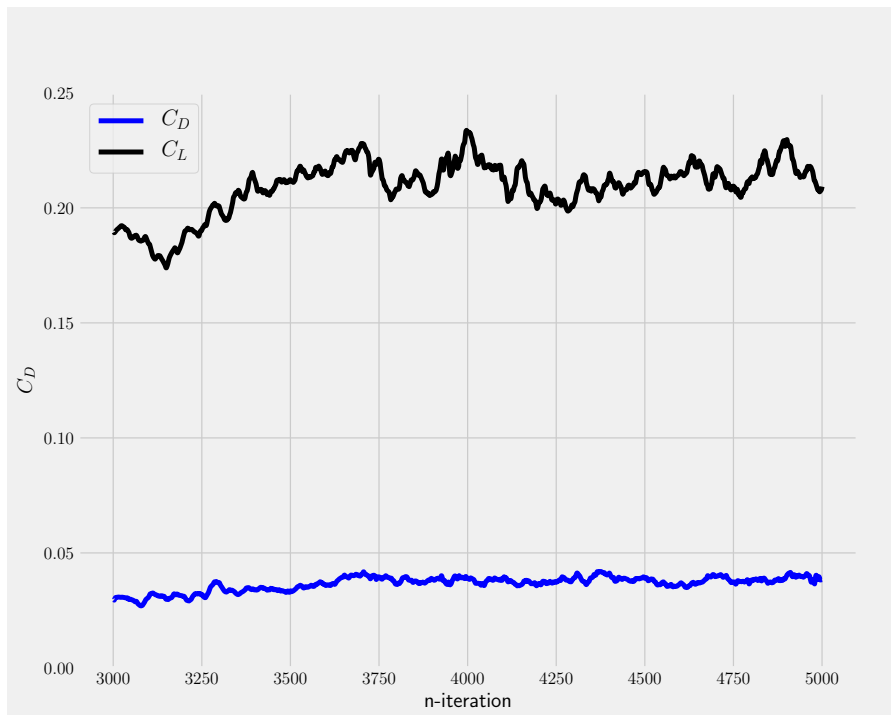


FIGURE 4.2: C_D values during iteration

estimated from the available polar drag airfoil. This is because the calculation only applies to the airfoil/wing, not the entire aircraft. Therefore, by using simulation, the C_{D_o} value appears at 0.0467.

Figure 4.2 shows that the drag coefficient appears in the area between 0.03 and 0.04. This value appears in the iterations from 3000 to 5000. And by plotting the drag coefficient due to the change in lift coefficient, Figure 4.3 shows the characteristics C_D value because C_L is convergent, the minimum C_D occurs when C_L is at 0 value.

4.3 Airfield Performance

Before starting airfield performance calculations, several variables need to be considered, the variables in Table 4.3 are obtained from the Table 1.8 in chapter 1 and the wing dimension in Table 1.5, those variables are: (Mcghee & Beasley, August 1, 1979)

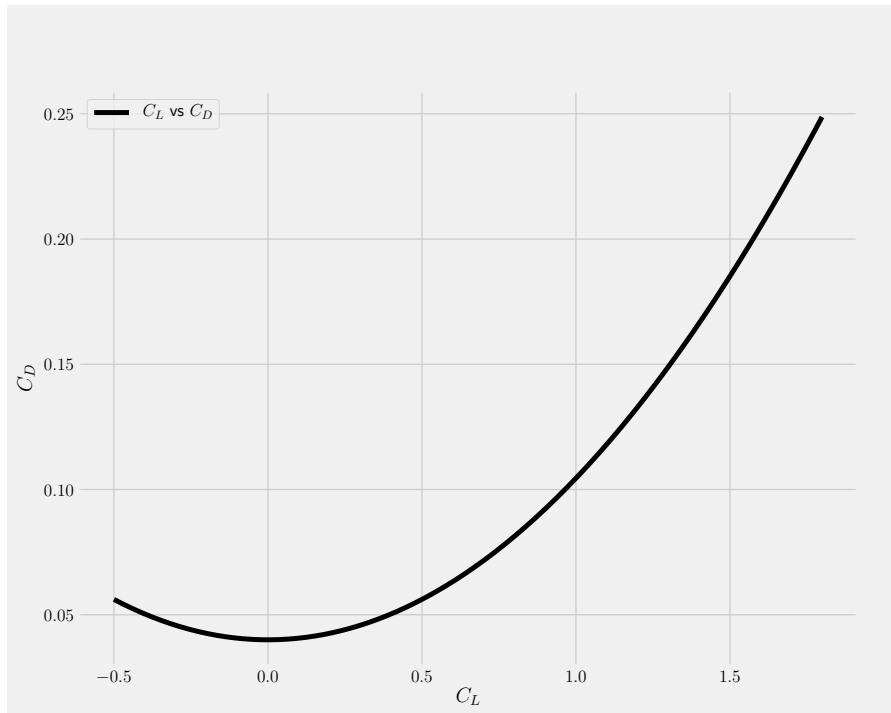


FIGURE 4.3: Drag polar of aircraft

TABLE 4.3: Performance Variables

| Variable | Value | Unit |
|------------------------------|----------|------|
| $C_{L\alpha}$ | 4.519 | /rad |
| $C_{L_{\max}}$ | 1.3411 | |
| μ_{asphalt} | 0.02 | |
| $\mu_{\text{brake system}}$ | 0.4 | |
| h | 0.100 08 | m |
| b (wingspan) | 1.916 | m |
| $\Phi(\text{Ground Effect})$ | 0.4112 | |

4.3.1 Take Off Ground Run

In the calculation of the take off ground run in Table 4.4, the required speed in the ground run phase is 20% higher than the stall speed, this applies to safety issues, therefore the ground run speed becomes 35 m s^{-1} . At this speed, the lift and drag show 242.021 N and 22.844 N. And the distance it takes GUAV-190417 to reach

TABLE 4.4: Take Off Performance

| Variable | Value | Unit |
|--------------------------|-----------|-------------------|
| $v_{LO} = 1.2v_{stall}$ | 35.3446 | m s^{-1} |
| $v_{stream} = 0.7v_{LO}$ | 24.741 23 | m s^{-1} |
| L | 242.0208 | N |
| D | 22.8445 | N |
| S_{LO} | 97.1046 | m |

the take off stage is 97 m.

4.3.2 Airborne Phase

TABLE 4.5: Airborne Performance

| Variable | Value | Unit |
|-----------------|----------|-------------------|
| v_{stall} | 29.4539 | m s^{-1} |
| n | 1.7139 | |
| R | 178.5445 | m |
| D | 29.3245 | N |
| $\sin \gamma c$ | 0.6434 | |
| γc | 0.6989 | rad |
| S_t | 114.87 | m |
| h_t | 41.8587 | m |

The airborne phase determined the data in Figure 4.5 where, the flight path aircraft radius from the liftoff to the climbing stage must have the same value. The prevailing radius in liftoff is 178 m with the angle formed of 0.64 radians or 36 degrees. Meanwhile, the distance required in this transition stage is 115 m, and the change in altitude is 42 m.

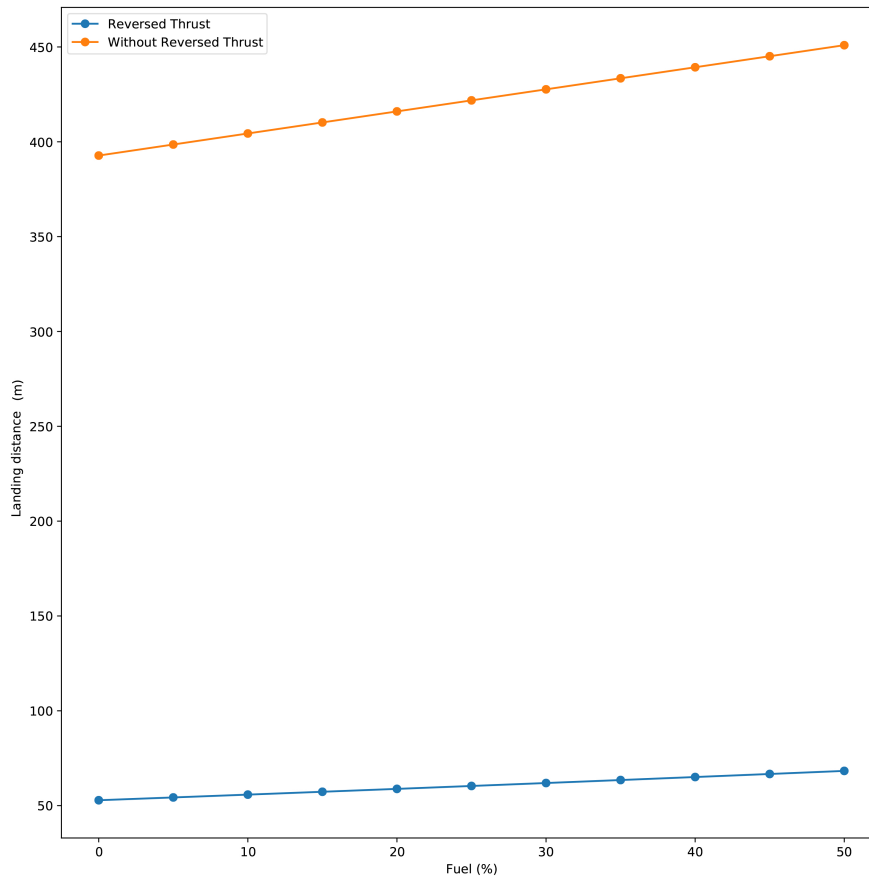


FIGURE 4.4: Landing distance performance due to Fuel Remaining

4.3.3 Landing Ground Run

In the landing ground run phase data in Table 4.4, the variation value applied to the remaining fuel. The range starts from 0% to 50%, which means that the amount of fuel starts from zero newtons to 39.2 N. By reducing the weight of the aircraft, the speed is also reduced. This proves that weight and speed are directly proportional. With reduced speed, the lift and drag forces also decrease.

For the landing distance, there are 2 cases applied. The first case is the distance required when the engine has a reverse thrust to assist braking which is shown by the blue line, while the second is without reverse thrust which is shown by orange line.

When the fuel remains as much as 50% or weighing 39.2 N, GUAV requires a path of 68.314m to land with the help of reversed thrust. Meanwhile, without

reversed thrust, GUAV requires a distance of 450.934 m. When the fuel tank is completely empty, the landing distance is 52.855 m with reversed thrust applied and 392.749 m without reversed thrust.

It can be concluded that the case that uses reverse thrust requires a shorter runway distance than without reverse thrust. With a lighter and less fuel capacity, the distance needed for an aircraft to landing is also shorter.

4.4 Climbing Performance

In climbing performance, 2 cases are applied and compared. The first case is the total weight used from a height of 0 to 22 000 m with the same value without reducing the fuel used. Whereas in the second case, the aircraft's total weight is reduced by the amount of fuel used to reach each altitude.

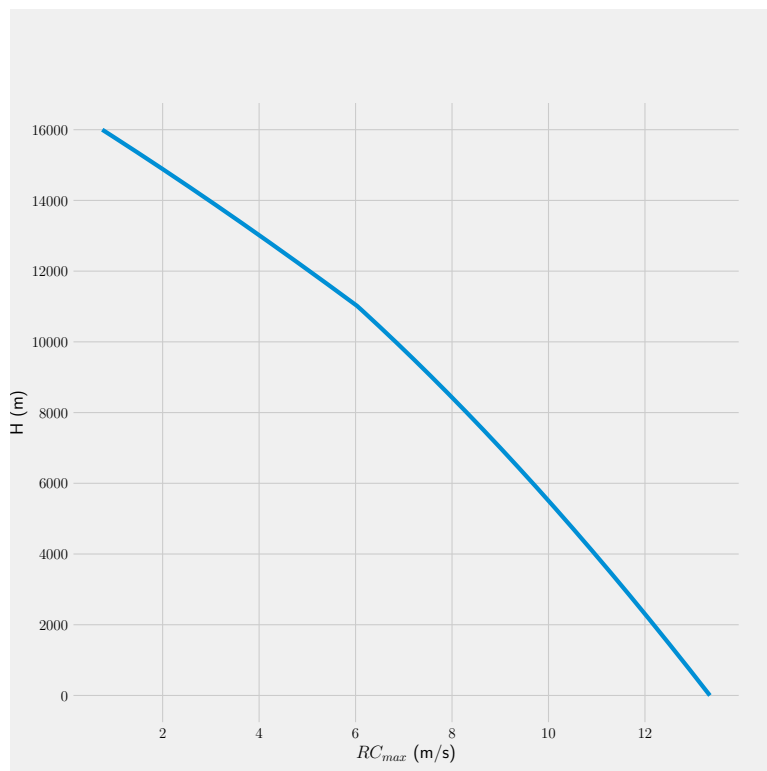


FIGURE 4.5: Maximum RC Characteristic due to Altitude with 200N Thrust Assumption

In the climbing performance calculation, by varying the altitude between 0 and 22 000 m above sea level, the air density will also be decreasing. Figure 4.5 explains that higher altitude results in smaller maximum rate of climb, correspondingly lower altitude cause a higher maximum rate of climb. This is because the air density is getting smaller and makes the plane's motion medium limited and more difficult. Therefore the velocity that applies to the aircraft is also getting smaller. The air density also affects an aircraft's thrust power. The higher altitude, the mediation of the engine thrust is also more tenuous. Therefore the maximum rate of climb value is decreasing.

It was found that GUAV-190417 has characteristic service ceilings around 15 800 - 16 000 m. Assuming the engine thrust applied is equal to 200 N and without fuel reduction calculation during take off, airborne, and climb phase. This altitude value is doesn't make sense if we compare it to commercial aircraft. But when this drone starts the first flight on 15 800 m, the drone can maintain its climb without losing its lift and not getting in a stall condition. However, because GUAV is designed with a fuel capacity of only 8 kg, so this aircraft can only touch an altitude around 4000 m without fuel weight reduction.

Figure 4.6 shows a change of behaviour from Figure 4.5. Since the climb rate is inversed, the linear relationship of both the rate of climb and altitude transforms exponentially. When the altitude of GUAV is getting higher, the maximum rate of climb inverse becomes higher. The minimum time to climb can be determined by calculating the area on the graph line's left side.

Figure 4.7 gives the result of the minimum time needed to reach a certain altitude. Where to reach 4000 m, GUAV needs at least 400 s of time consumption. And for reaching the altitude of 16 000 m, GUAV needs at least 3000 s or equal to 50 min. The time needed value become make sense by referring to 4.8, where the endurance that can be obtained by a full tank GUAV (weight ratio = 1.25) is 89 min.

Figure 4.9 shows that the power required and power available result corresponds to airspeed in altitude variations. The solid line represents the power required, and the dashed line represents the power available. From this table, we can analyze that GUAV needs a bigger power available and required than higher altitude in lower altitude.

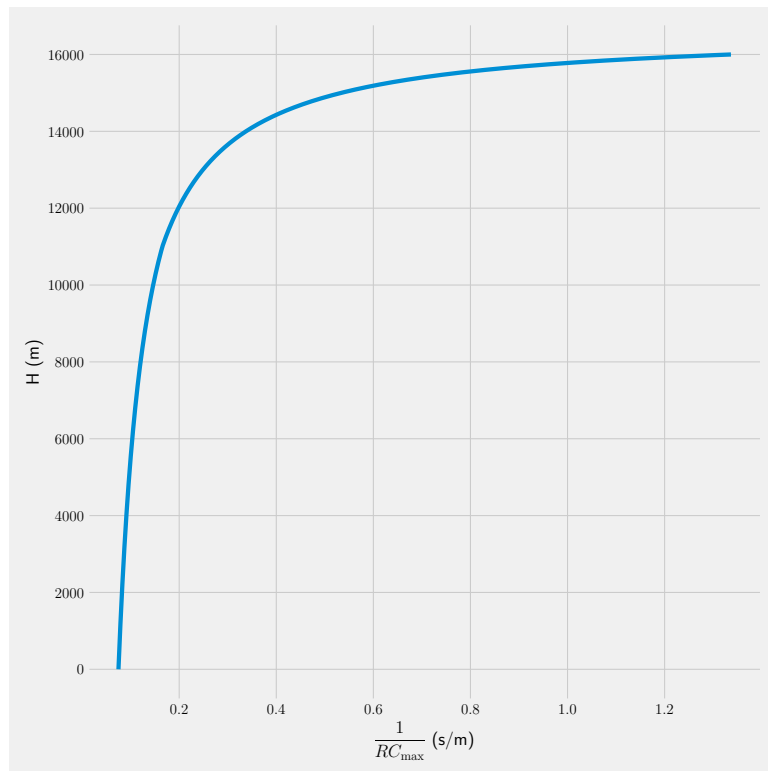


FIGURE 4.6: Maximum RC inverse Characteristic due to Altitude

The maximum velocity during climbing also can be determined by defining the maximum excess power where excess power is equal to the power available minus the power required. Figure 4.9 shows that the maximum velocity at the lower altitude has a smaller value than the higher altitude.

In Figure 4.10, five lines represent the rate of the climb due to the speed at different altitudes. There are a total of 5 types of heights. The blue lines show during sea-level altitude behavior, followed by altitudes at 4 km, 8 km, 12 km, and 16 km.

At the sea level altitude, blue line behavior, the rate of climb is increasing while the increased airspeed. But when the rate of climb reaches the maximum point, the value gets decreases. This result also has the same pattern at 4 km until 16 km. However, the value of the maximum rate of climb decreases with increasing altitude.

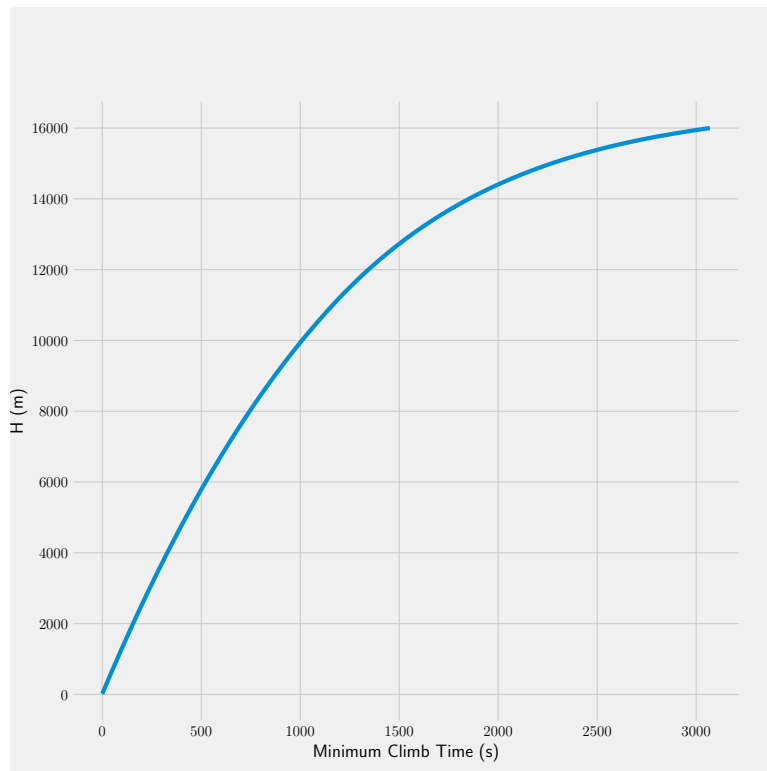


FIGURE 4.7: Minimum Time Needed

4.5 Gliding Performance

In gliding performance, the result is shown in Figure 4.11, 4.12 and 4.13, the variations in angle of attack are implemented from -3.35 to 17 degree. By varying this value, the lift coefficient, drag coefficient, the ratio C_L/C_D and C_L^3/C_D^2 can be calculated. These variables are used to calculate the angle of descent, rate of descent, and velocity during gliding. Then plotting is done become a hodograph between velocity with rate of descent. For the hodograph, the amount of MTOW varies from 0.1MTOW , 0.3MTOW , 0.5MTOW , 0.8MTOW and MTOW .

In Figure 4.13, each line is shown the same pattern, where if we draw a line from 0 points (origin tangent) to one of the curves, the line will create a velocity flight path. The degree between v_C and the velocity flight path will be defined as a degree of descent. The rate of descent is getting bigger with the increased horizontal speed, but when the horizontal speed reaches the maximum value, the descent rate decreases. There are four variations of altitude, where at higher altitude, the rate

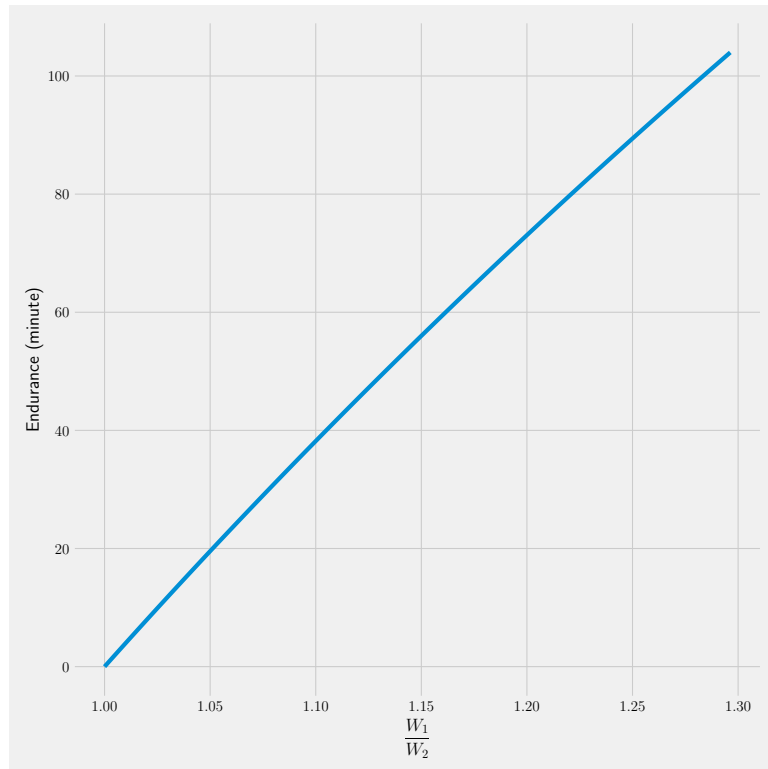


FIGURE 4.8: GUAV Endurance (Syauqi, 2021)

of descent and horizontal velocity have the greatest value compared to other levels. Meanwhile, if the MTOW decreases in number, the rate of descent and horizontal velocity also decreases.

TABLE 4.6: Gliding Performance at 4000 m altitude

| Variable | Value | Unit |
|------------|--------|------|
| t_{\max} | 800 | s |
| | 13.33 | min |
| R_{\max} | 38 414 | m |
| | 38.414 | km |

Table 4.6 shows the maximum time needed and range maximum that GUAV can reach. At 4000 m altitude above sea level, GUAVs can glide for 13.33 min with minimum rate of descent applied. And by minimum degree of descent GUAV may glide as far as 38.414 km.

PERFORMANCE REVIEW AND ANALYSIS OF GUAV-190417 TARGET DRONE:
AIRFIELDS, SYMMETRIC CLIMB, AND GLIDING

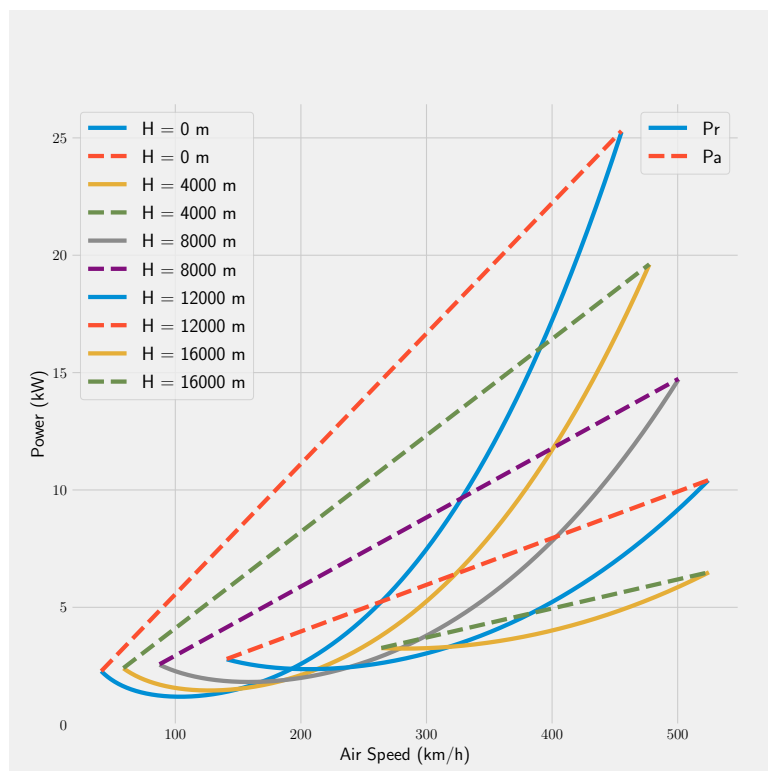


FIGURE 4.9: Performance Diagram

PERFORMANCE REVIEW AND ANALYSIS OF GUAV-190417 TARGET DRONE:
AIRFIELDS, SYMMETRIC CLIMB, AND GLIDING

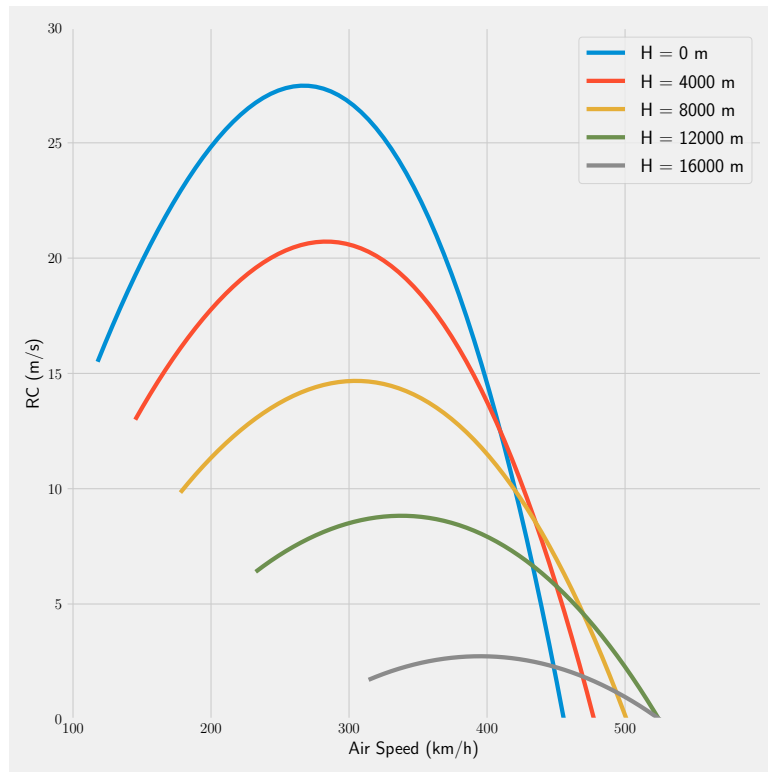


FIGURE 4.10: RC Characteristic Due to Velocity in Various Altitude

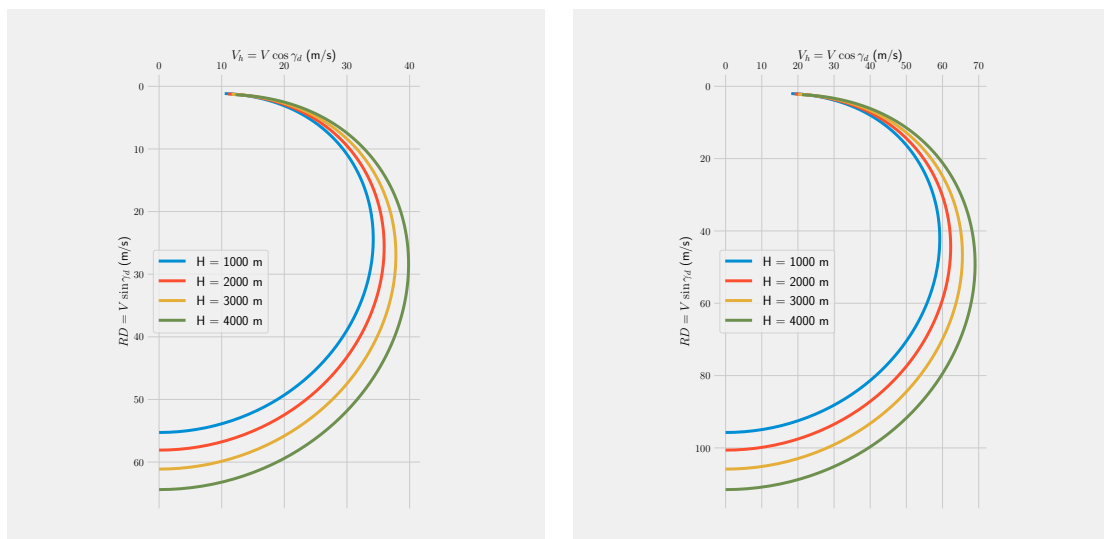


FIGURE 4.11: Gliding Hodograph with 0.1 and 0.3 MTOW

PERFORMANCE REVIEW AND ANALYSIS OF GUAV-190417 TARGET DRONE:
 AIRFIELDS, SYMMETRIC CLIMB, AND GLIDING

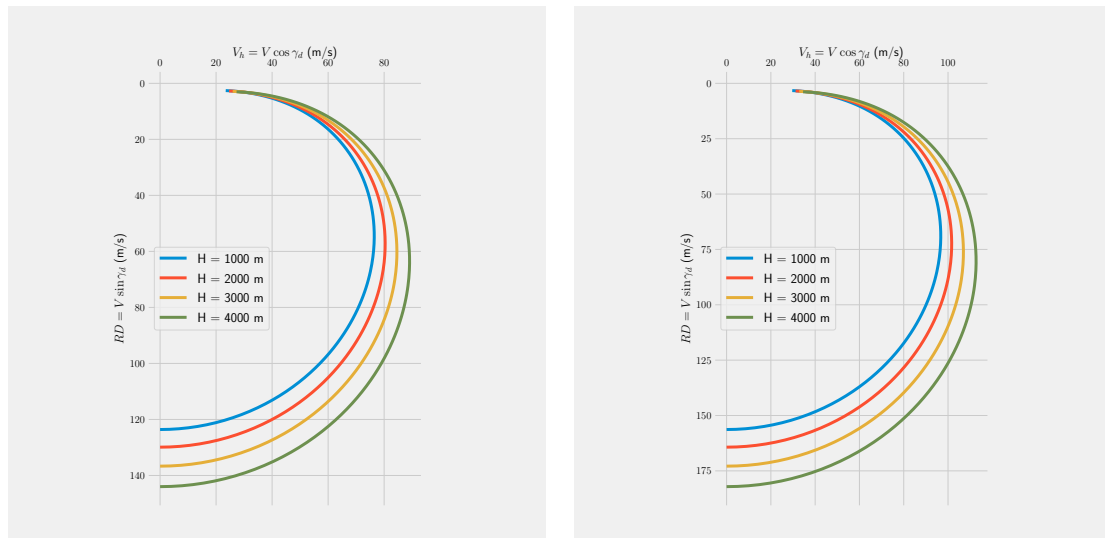


FIGURE 4.12: Gliding Hodograph with 0.5 and 0.8 MTOW

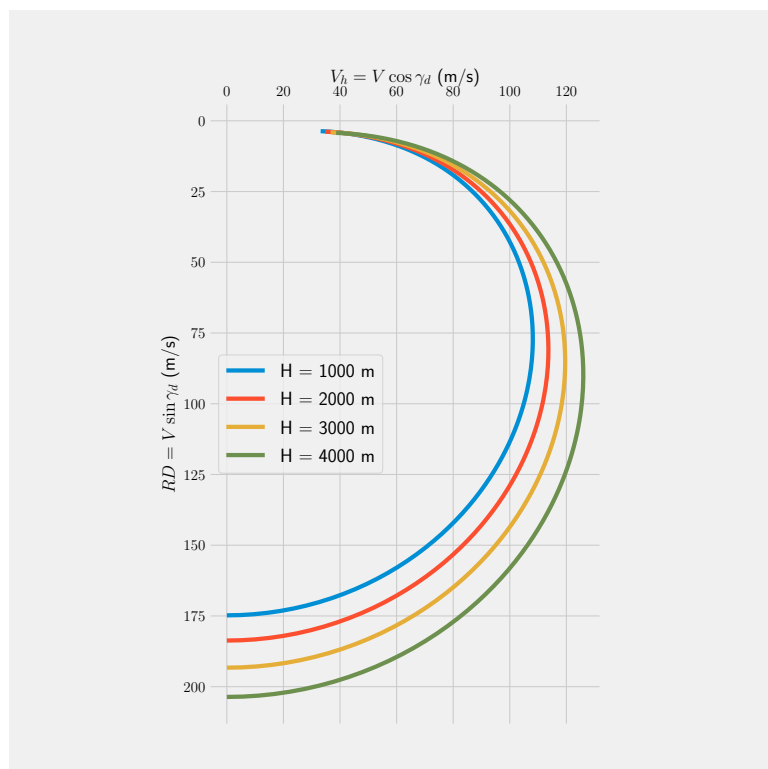


FIGURE 4.13: Gliding Hodograph MTOW

CHAPTER 5

SUMMARY, CONCLUSION, RECOMMENDATION

5.1 Conclusion

This work's main purpose is to analyze the GUAV-190417 design to proceed to the prototype, production, and testing stages. The determination of whether the design is qualified or not is by taking into account the performance in each phase. These results include:

1. Aerodynamics design review:

Through open foam software, the lift coefficient value at 0 degrees appears in the number 0.3826 and for parasite drag of the whole body is 0.0467. Meanwhile, through calculations using the $C_{L\alpha}$ graph, the resulting C_L value is 0.3529, where this result is not much different from the simulation results.

2. Airfield Performance:

- Take-off ground run: The distance that GUAV needs to take off is 97.105 m.
- Airborne phase: A horizontal distance of 114.87 m is required for the transition from lift off to climbing phase, and the altitude change that occurs is 41 859 m above sea level.
- Landing ground run: When the fuel remains as much as 50% or weighing 39.2 N, GUAV requires a path of 68.314 m to land with the help of reversed thrust. Meanwhile, without reversed thrust, GUAV requires a distance of 450.934 m. When the fuel tank is completely empty, the landing distance is 52.855 m with reversed thrust applied and 392.749 m

without reversed thrust. Therefore, it can be concluded that the fewer fuel remains have a shorter landing distance needed.

3. Climbing Performance:

GUAV has an service ceilings value between 15 800 m and 16 000 m with at least 89 min. Meanwhile, with a capacity of GUAV that can accommodate 8 kg of fuel, GUAV is only able to reach an altitude of 4000 m with the time needed for 400 s. The rate of climb is increasing while the increased airspeed. But when the rate of climb reaches the maximum point, the value of RC gets decreases while the increased airspeed.

4. Gliding Performance:

In the gliding phase, the rate of descent is getting bigger with the increased horizontal velocity, but when the horizontal speed reaches the maximum value, the descent rate decreases. At higher altitude, the rate of descent and horizontal velocity have the greatest value compared to other levels. Meanwhile, if the MTOW decreases in number, the rate of descent and horizontal velocity also decreases. GUAV with MTOW applied can glide for 13.33 min with minimum rate of descent applied. And by minimum degree of descent GUAV may glide as far as 38.414 km at 4000 m altitude.

5.2 Recommendation

Although this work has shown the UAVs conceptual and preliminary design legitimacy, it still has many rooms for improvement. Future work can be developed upon this research. Such possibilities are listed below:

- An optimal value of lift coefficient and drag polar can be achieved by optimizing a target drone's configuration, airfoil type, and aspect ratio of wing dimension.
- To complete the design review before entering a detailed design, the structure of GUAV-190417 can be analyzed to strengthens the resistance of pressure and reduces damage to the entire aircraft body.

- The stability and control of GUAV-190417 can be analyzed and calculated. This works to ensure the aircraft can hold constant incidence, have a high maneuverability characteristic, and run smoothly by the pilot.
- The methodology and calculations carried out in this work can be implemented into the target drones performance analysis powered by a supersonic jet engine.

References

- Anderson, J. (2011). *Fundamentals of aerodynamics*. New York: McGraw-Hill.
- Anderson, J. D. (1998). *Aircraft performance & design*. MCGRAW HILL BOOK CO. Retrieved from https://www.ebook.de/de/product/3648745/john_d_anderson_aircraft_performance_design.html
- Anderson, J. D. (2015). *Introduction to flight*. PAPERBACKSHOP UK IMPORT. Retrieved from https://www.ebook.de/de/product/24169507/john_d_anderson_introduction_to_flight.html
- Francis J. Hale, H. (1984). *Introduction to aircraft performance, selection and design*. John Wiley & Sons, Inc. Retrieved from https://www.ebook.de/de/product/3635027/francis_j_hale_hale_introduction_to_aircraft_performance_selection_and_design.html
- Mccormick. (1994). *Aerodynamics, aeronautics, and flight mechanics*. John Wiley & Sons. Retrieved from https://www.ebook.de/de/product/3635471/mccormick_aerodynamics_aeronautics_and_flight_mechanics.html
- Mcghee, R. J., & Beasley, W. D. (August 1, 1979). *Low-speed aerodynamic characteristics of a 13 percent thick medium speed airfoil designed for general aviation applications* [patentus]. Retrieved from <https://ntrs.nasa.gov/citations/19810003507>
- Nicolai, L. (2010). *Fundamentals of aircraft and airship design*. Reston, Va: American Institute of Aeronautics and Astronautics.
- OpenFoam. (2012). *The open source cfd toolbox*. Creative Commons Attribution - Non Commercial No Derivs 3.0 Unported License. Retrieved from <https://www.openfoam.com/documentation/>
- Raymer, D. (1989). *Aircraft design : a conceptual approach*. Washington, D.C: American Institute of Aeronautics and Astronautics.
- Ruijgrok, G. J. J. (2009). *Elements of airplane performance*. Place of publication not identified: Vssd Pub.

- Sadraey, M. H. S. (2012). *Aircraft design*. John Wiley & Sons. Retrieved from https://www.ebook.de/de/product/18698777/sadraey_mohammad_h_sadraey_aircraft_design.html
- Syauqi, R. (2021). Performance review and analysis of guav-190417 target drone: Cruising and turning.
- Torenbeek, E. (2010). *Synthesis of subsonic airplane design*. Springer Netherlands. Retrieved from https://www.ebook.de/de/product/13447844/e_torenbeek_synthesis_of_subsonic_airplane_design.html
- Valavanis, K. P. (2014). *Handbook of unmanned aerial vehicles*. SPRINGER NATURE. Retrieved from https://www.ebook.de/de/product/11883304/handbook_of_unmanned_aerial_vehicles.html

Appendices

Turnitin Report

PERFORMANCE REVIEW AND ANALYSIS OF GUAV-190417 TARGET DRONE: AIRFIELDS, SYMMETRIC CLIMB, AND GLIDING

ORIGINALITY REPORT

2%

SIMILARITY INDEX

1%

INTERNET SOURCES

1%

PUBLICATIONS

0%

STUDENT PAPERS

PRIMARY SOURCES

- 1 "The Proceedings of the 2018 Asia-Pacific International Symposium on Aerospace Technology (APISAT 2018)", Springer Science and Business Media LLC, 2019
Publication <1%
- 2 Mario Asselin. "An Introduction to Aircraft Performance", American Institute of Aeronautics and Astronautics (AIAA), 1997
Publication <1%
- 3 archive.org
Internet Source <1%
- 4 Bandu N. Pamadi. "Performance, Stability, Dynamics, and Control of Airplanes, Second Edition", American Institute of Aeronautics and Astronautics (AIAA), 2004
Publication <1%
- 5 Submitted to Georgia Institute of Technology Main Campus
Student Paper <1%

Curriculum Vitae



| Basic Information | |
|-------------------|---|
| Name | Jordan Yap Hong Yong |
| Place of Birth | DKI Jakarta, Indonesia |
| Date of Birth | 12 July 1999 |
| Address | Teluk Gong, Jalan A1 No.65, Jakarta-Utara 14450 |

| Year | Education |
|-----------|--|
| 2017-2021 | International University Liaison Indonesia |
| 2014-2017 | SMAK IPEKA PLUIT |

| Year | Work Experiences and Workshop |
|------|---|
| 2019 | Maintenance Planning and Control Intern upon Sriwijaya Air, Indonesia |
| 2020 | Basic Finite Element Analysis Workshop by PT Aerozeta Engineering |

| Year | Organization Experience |
|-----------|---|
| 2019-2020 | President of Aviation Engineering Student Association |
| 2018-2019 | Member of Aviation Engineering Student Association |
| 2017-2020 | President of IULI Basketball Extracurricular |

| Year | Activities |
|------|---|
| 2021 | Moderator of IULI Info Sharing |
| 2019 | Participant of Higher Education for Aviation Profession Seminar by EASA |
| 2019 | Event Committee of New Student Orientation Week IULI |
| 2018 | President of IULI Student Executive Board General Election |

PERFORMANCE REVIEW AND ANALYSIS OF GUAV-190417 TARGET DRONE:
AIRFIELDS, SYMMETRIC CLIMB, AND GLIDING

2018 President of Basketball Division IULI Internal Cup

Language Skill

Indonesian Mother Tongue

English Intermediate

Mandarin Intermediate

German Beginner
